Politecnico di Torino

Laurea Magistrale in
INGEGNERIA DEI MATERIALI PER L'INDUSTRIA 4.0
Collegio di Ingegneria Chimica e dei Materiali

A.a. 2024/2025
July

Impact of Surface Post-Treatments on the Properties of Additively Manufactured Ti-6242 Alloy

Supervisor:
Prof. Abdollah Saboori

Candidate:
Mahta Khorramian

Acknowledgement

I would like to express my heartfelt gratitude to Professor Abdollah Saboori. His unconditional support, exceptional patience, and deep belief in my abilities have shaped this journey in ways I will never forget. From the beginning, he saw potential in me—sometimes even before I saw it myself—and gave me the freedom and encouragement to grow into it. His mentorship has been a guiding light, not just academically but personally, and I will always be grateful for the trust he placed in me, the lessons he shared, and the confidence he helped me build.

A special thank you to the Integrated Additive Manufacturing (IAM) center, led by Professor Luca Iuliano, for fostering a collaborative and innovative research space. The hands-on experiences within the lab have enriched my understanding of additive manufacturing immensely. I'm especially grateful to the researchers and fellow students for their technical support, insightful contributions, and constant encouragement throughout this journey.

I would also like to extend my sincere thanks to the Politecnico di Torino, the Department of Applied Science and Technology, and its dedicated faculty for providing an outstanding academic environment that has nurtured my development. Being part of such a forward-thinking and supportive institution has been a true privilege.

To my friends and family, your love, patience, and steady encouragement have been the emotional foundation behind this achievement. Thank you for always being there, reminding me of my strength, and pushing me to keep going.

This work is the result of many generous and kind people who believed in me. I feel truly fortunate to have walked this path with your support.

Thank you, from the bottom of my heart.

Abstract

Metal additive manufacturing, particularly Laser Powder Bed Fusion (L-PBF), enables the fabrication of geometrically complex components such as those made from Ti-6Al-2Sn-4Zr-2Mo (Ti-6242). However, the as-built surface condition often exhibits high roughness and partially fused particles, which can negatively impact part life and wear resistance. This study focused on optimizing L-PBF process parameters to maximize relative density and minimize defects, followed by a comprehensive evaluation of mechanical, thermal, and chemical base surface post-treatment techniques: grinding, tumble finishing, laser polishing, and chemical polishing. Process optimization identified a parameter set—200 W laser power, 1000 mm/s laser scan speed— that achieved the highest density (~99%) and relatively low surface roughness, selected as the baseline for surface treatment trials. All post-processing methods significantly reduced surface roughness, with grinding achieving the greatest reduction, followed by tumble finishing, laser polishing, and chemical polishing. SEM analysis and roughness profiling revealed distinct mechanisms of surface modification, including plastic deformation, abrasive smoothing, and localized melting. Nanoindentation tests indicated that laser polishing slightly reduced near-surface hardness due to thermal relaxation, while tumble finishing caused localized strain hardening. These results highlight the importance of combining optimized build parameters with tailored surface finishing strategies to enhance the performance of Ti-6242 AM components, particularly for applications demanding high surface integrity and mechanical reliability.

Keywords:

Additive Manufacturing; Laser Powder Bed Fusion (L-PBF); Ti-6242; Surface Post-Treatment; Surface Roughness; Nanoindentation; Process Optimization

Contents

Figures

Tables

Table of Abbreviations

AcAl	Acid-Alkali (surface treatment)
AM	Additive Manufacturing
bcc	Body-Centered Cubic
BJ	Binder Jetting
CASE	Chemically Assisted Surface Enhancement
CP	Cavitation Peening
DED	Directed Energy Deposition
EB-PBF	Electron Beam Powder Bed Fusion
ECP	Electrochemical Polishing
EP	Electropolishing
hcp	Hexagonal Close-Packed
HIP	Hot Isostatic Pressing
HT	Heat Treatment
ISF	Isotropic Superfinishing
L-PBF	Laser Powder Bed Fusion
LSP	Laser Shock Peening
ME	Material Extrusion
MJ	Material Jetting
PBF	Powder Bed Fusion
Ra	Arithmetic Mean Surface Roughness
Rz	Average Height of the Profile
SB	Sand/Bead Blasting
SBF	Simulated Body Fluid
SHL	Sheet Lamination
SP	Shot Peening
SSE	Stair-Stepping Effect
TF	Tumble Finishing
Ti-6242	Titanium-6Aluminum-2Tin-4Zirconium-2Molybdenum
Ti6Al4V	Titanium-6Aluminum-4Vanadium
UNSM	Ultrasonic Nano-Crystal Surface Modification
VP	Vat Photopolymerization
WAAM	Wire Arc Additive Manufacturing

1 Introduction

1.1 State of the Art

Titanium alloys are materials with exceptional corrosion, mechanical properties, and biomedical compatibility, making them ideal for a range of applications, including biomedical implants[1], [2], aerospace[3], automotive[4], and high-temperature environments where creep resistance is essential[5]. However, one notable disadvantage of titanium alloys is their high cost [6], [7]. Also, the constraints of conventional manufacturing methods like casting, rolling, and forging challenge the use of titanium alloys[8]. Due to the strong reactivity of liquid titanium with mold sands, the materials have mostly not been cast by traditional methods [9], [10]. There is insufficient information available about the AM of Ti-6242 alloy, despite the fact that the AM of Ti6Al4V alloy has been the subject of numerous studies [11], [12], [13]. Although this particular alloy is known for its promise in high-temperature applications, its use in AM has not been fully explored. The as-built laser powder bed fusion (L-PBF) produced Ti-6242, for instance, has been reported to have an outstanding ultimate tensile strength of 1437 MPa at room temperature [14].

Additionally, the low thermal conductivity of titanium alloys poses inherent challenges in machining, leading to elevated cutting temperatures [15]Further, the spring-back characteristics of these alloys complicate their forming process at room temperature, even when they are annealed [16], [17]. As a result, industries are investing in AM techniques to increase productivity and cut expenses while maintaining the superior benefits of titanium alloys [18], [19]. Titanium alloys are typically available in both powder and wire forms, making them suitable feedstock candidates for all major categories of metal AM [20], [21]. AM processes are diverse, with directed energy deposition (DED) and powder bed fusion (PBF) being the two main methods for printing titanium alloys. Laser powder bed fusion (L-PBF) and electron beam powder bed fusion (EB-PBF) are two typical PBF metal printing processes. DED utilizes lasers, electron beams, or electric arcs to melt metal powders or wires that are deposited along printed paths [22], [23].

All additive manufacturing processes mentioned commonly face challenges with surface quality compared to traditional manufacturing. The layer-by-layer deposition and complex thermal dynamics often lead to uneven and irregular surface features [24]. Contributing factors include feedstock properties, part design, and process parameters. Common causes of roughness are the stair-step effect, partially fused particles (especially in PBF), spatters, and melt pool instability due to wetting behaviors [25]. Surface orientation, geometry, and support structure design also impact surface roughness, e.g., down-skin surfaces and shallow angles generally result in rougher finishes. These imperfections not only reduce dimensional accuracy but can serve as stress concentrators, promoting early failure. Process variables such as powder morphology and deposition settings

significantly affect surface roughness[26], [27]. As surface condition critically affects mechanical performance, post-processing treatments are essential for improving consistency and functionality [28], [29]. Techniques range from material removal to surface patterning, each targeting enhanced surface regularity. Despite advancements, optimizing post-processing methods, improving scalability, and minimizing side effects remain key challenges. This study explores four different surface post-treatment chemical, mechanical, and thermal base post-treatment strategies, including grinding, tumble finishing (TF), chemical polishing and laser polishing, and investigates and discusses the effect of these treatments on the surface and sub-surface of the L-PBF parts out of Ti-6242 alloy.

1.2 Ti-6242

Titanium alloys have garnered more attention in recent years because of their expanding applications, such as in the automotive and biomedical sectors.[30], [31]. As demonstrated in Figure 1, Ti exists as α-Ti with a hexagonal close-packed (hcp) structure below the β-transus temperature and transforms to β-Ti with a body-centered cubic (bcc) structure above this temperature. The phase transformation temperature of Ti can be greatly impacted by the addition of certain alloying elements[32] . Ta, Mo, and Nb are examples of β-stabilizers that can lower the β/α transit temperature, whereas α-stabilizers like Al, C, and O can typically raise it [33]. Thus, Ti alloys can be classified into five crystalline categories of α, near α, α +β, near β, and β types, contributing desirable and versatile combinations of excellent mechanical and chemical properties [[34], [35].

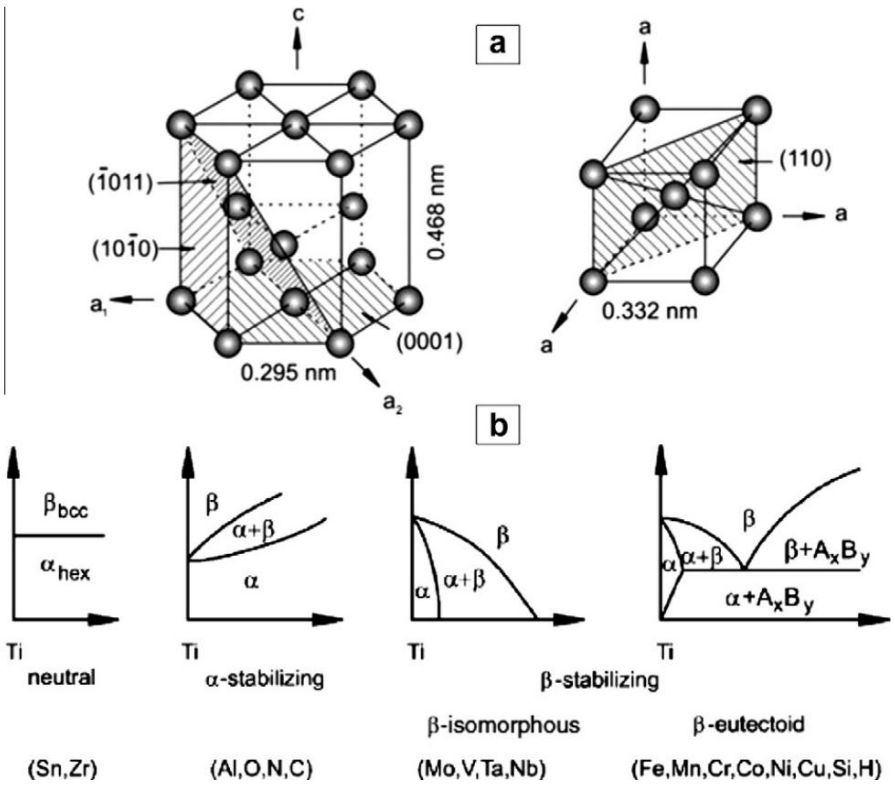

Figure 1 (a) The hcp (alpha) and bcc (beta) structure of titanium. (b) Categories of titanium phase diagrams formed with different alloying additions.[36]

One of these alloys, Ti6Al4V, belongs to the α + β titanium family and has become an important driver in the titanium industry because of its remarkable specific strength, good corrosion resistance, and resistance to fatigue and creep [3,4]. Ti–6Al–2Sn–4Zr–2Mo alloy, also known as Ti-6242, the near α Ti-alloy, is another notable member of the titanium alloy family [5,6]. Ti-6242 has a greater working temperature than the commonly used Ti6Al4V, which has a limited working temperature of less than 400 °C. Ti-6242 is ideal for applications involving temperatures up to 540 °C and has exceptional creep resistance [[5], [6], [7], [8]]. Moreover, although β titanium alloys are known to demonstrate excellent corrosion behavior, specifically in biomedical applications such as in simulated body fluid, they usually exhibit lower strength than their counterparts in other titanium families. For example, the Ti-6242 alloy exhibits a substantially better strength than the β Ti–35Nb–7Zr–5Ta alloy. [[37], [38], [39]].

Table 1 Ti-6242 data sheet [40], [41], [42]

Physical Properties	Metric	Comments
Density	4.54 g/cc	
Mechanical Properties		
Hardness, Brinell	304	Estimated from Rockwell C.
Hardness, Knoop	330	Estimated from Rockwell C.
Hardness, Rockwell C	32	
Hardness, Vickers	318	Estimated from Rockwell C.
Tensile Strength, Ultimate	940 MPa	
Tensile Strength, Yield	860 MPa	
Elongation at Break	15 %	
Modulus of Elasticity	113.8 GPa	
Compressive Yield Strength	1070 MPa	
Notched Tensile Strength	1170 MPa	K_t (stress concentration factor) = 3.0
Ultimate Bearing Strength	2000 MPa	e/D = 2
Bearing Yield Strength	1620 MPa	e/D = 2
Poisson's Ratio	0.32	
Charpy Impact	20 J	V-notch
Fatigue Strength	280 MPa	at 1E+7 cycles. K_t (stress concentration factor) = 3.0
Fatigue Strength	480 MPa	1E+7 cycles, Unnotched
Shear Modulus	43.1 GPa	Calculated
Shear Strength	660 MPa	Ultimate shear strength
Electrical Properties		
Electrical Resistivity	0.00019 ohm-cm	
Thermal Properties		
CTE, linear 20°C	7.7 µm/m-°C	20-100ºC
CTE, linear 250°C	8.1 µm/m-°C	Average over the range 20-315ºC
CTE, linear 500°C	8.1 µm/m-°C	Average over the range 20-540ºC
Specific Heat Capacity	0.46 J/g-°C	
Thermal Conductivity	7.1 W/m-K	
Melting Point	Max 1700 °C	Liquidus: Estimated from similar materials
Liquidus	1700 °C	Estimated from similar materials
Beta Transus	990 °C	

However, it is frequently acknowledged that these titanium alloys' great strength, chemical reactivity, and low heat conductivity make them difficult to machine in the case of complex geometries. [[43], [44]].

1.3 Additive Manufacturing

The basic idea behind all AM technologies is to slice a solid model into several layers, make a tool path for each layer, upload the data to the machine, and then use a heat source (such as a laser, electron beam, electric arc, or ultrasonic energy) and feed stock (such as metal powder, wire, or thin metal sheet) to build the part up layer by layer while adhering to the sliced model data. According to ASTM F2792-12a, all AM technologies fall into one of seven general categories: Vat photopolymerization (VP), Material Extrusion (ME), Material Jetting (MJ), Binder Jetting (BJ), PBF, DED, and Sheet Lamination (SHL). [45] Of these seven categories, only four involve metal processing—DED, PBF, SHL, and BJ—and mostly the first three of these four have been employed for processing titanium and its alloys.[46] Unlike BJT and SHL, PBF and DED can create a net-shaped part straight from a computer model without the need for extra processing steps to get the desired form [47]. PBF and DED techniques vary according to the heat source (which can be a laser, electron beam, plasma arc, or gas metal arc) and feedstock (wire or powder). Reactive metals can be used in electron beam operations since they are carried out in a vacuum or low-pressure inert gas environment. Conversely, some heat sources require the use of an inert gas to insulate the components [47].

1.3.1 DED

DED is gaining popularity since its mechanical characteristics are like those of conventional manufacturing methods. Using focused heat energy, such as a laser, electron beam, or plasma arc, DED is an AM technique that forms solid three-dimensional (3D) structures by liquefying and placing materials. DED is gaining popularity since its mechanical characteristics are similar to those of conventional manufacturing methods. Using focused heat energy, such as a laser, electron beam, or plasma arc, DED is an AM technique that forms solid three-dimensional (3D) structures by liquefying and placing materials. stacking layers [48]. Compared to subtractive production, this manufacturing technique is quicker and more economical. It can create complex parts with little loss of materials. Additionally, DED is incredibly effective when used for remanufacturing and repair[49]. As shown in Figure 2, DED may be divided into two groups according to the feedstock that is utilized: wire feed DED and powder feed DED. In the wire feed system, the wire is fused to the substrate using a laser or arc, whereas in the powder feed system, the material is melted during the deposition process. The feedstock is concurrently deposited onto the substrate for the first layer or the prior layer by the focused energy source. By melting the source material and the

layer in front of it, a melt pool is created during this process. As the material cools, the resultant deposition bead forms. [50]

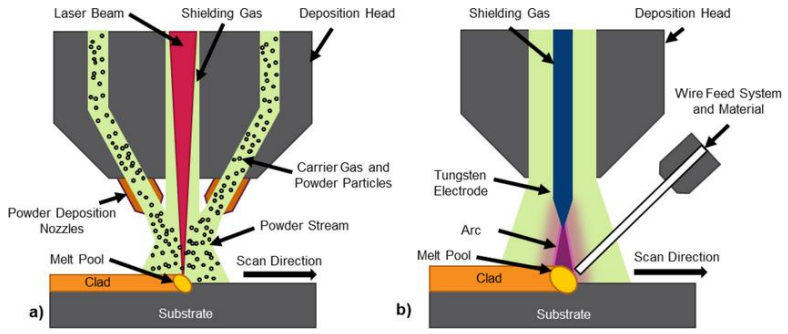

Figure 2 Schematic of DED processes a) powder-fed DED and b) wire-fed DED [51]

Powder feed DED offers better printing accuracy than wire feed DED, albeit at a relatively slower printing pace. DED still has challenges in achieving acceptable surface finishes and reducing porosity and cracks in the generated component, despite its significant benefits over other metal additive manufacturing processes[52]. A number of factors, including trapped gas, inadequate fusion, rapid solidification, and inadequate powder melting, can result in microstructural flaws [53]. A significant challenge for the growing DED industry is the broad variety of component quality. Defect generation, laser-material interactions, and process parameters are some of the factors that affect this variability.[54]

1.3.2 PBF

PBF techniques utilize either electron or laser beam power to melt specific areas of each thin layer within a pre-deposited powder bed, enabling the fabrication of products. [[55], [56], [57]] There are two main categories of PBF based on the type of heat source used: electron beam PBF (EB-PBF) and laser PBF (L-PBF).

1.3.2.1 EB-PBF

An electron beam is used as the heat source in the EB-PBF technique. In this method, free electrons are controlled and guided by electric and magnetic fields to create a focused beam in a vacuum. Heat is produced when a high-velocity electron beam collides with a substance. This high temperature can effectively melt electrically conducting materials when it is concentrated. EBM should be performed in a vacuum chamber since electrons scatter and disperse when they come into contact with gas atoms between the electron gun and the material being heated. Vacuum (10^4–10^5 mbar) is used in the process, which is essential for metals and alloys that are very susceptible to gases like oxygen and nitrogen.[58] Next, to limit electrostatic charging and smoke problems, a small helium pressure of 10 3 mbar is applied[59], [60]. The manufacturing rate is increased by EBM's special characteristics, which enable the fabrication of almost fully dense

components in a single printing job. A build file has been sliced, optimized, and posted into the EBM system, as seen in Figure 3. Before melting the powder via contour melting or hatch melting, respectively, a powerful electron beam warms the powder bed to the optimal temperature. The built environment stays hot, occasionally surpassing 1000°C, which leaves few residual stresses and allows for the processing of materials that are prone to cracking. Furthermore, residual stresses in EBM are significantly smaller than in L-PBF due to the greater bed temperature. Notably, EBM sets itself apart by producing components with low internal tensions [61]

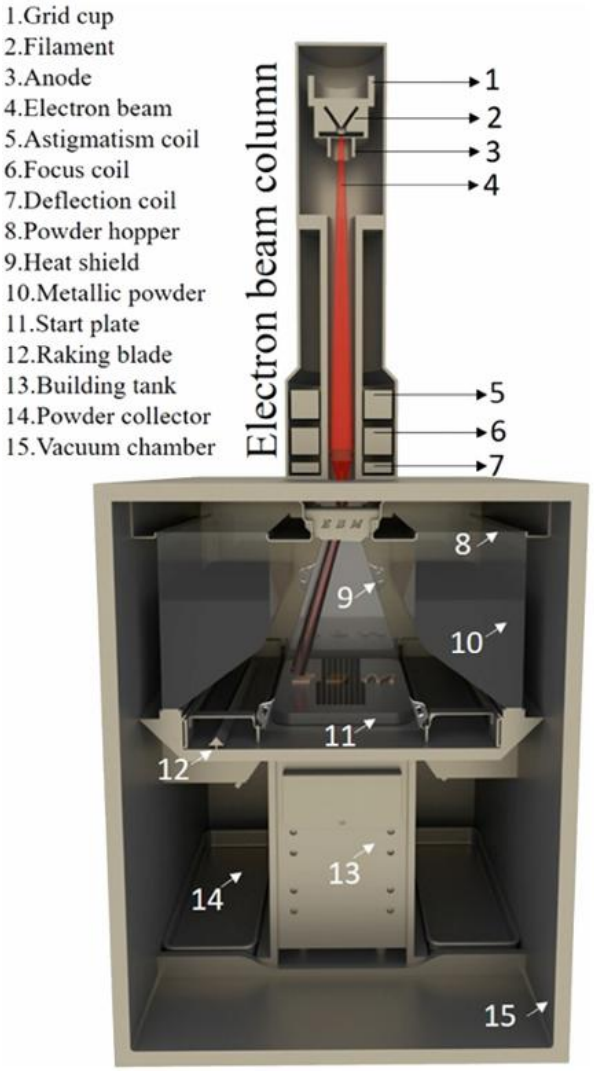

Figure 3 Principal schematic of the EBM machine.[30]

1.3.2.2 L-PBF

One of the most important direct AM techniques is L-PBF, which enables the creation of products with intricate internal structures and unique shapes.[60,61] The L-PBF techniques use a high-energy-density laser beam to selectively melt a thin layer of powder that has been applied to a base plate in accordance with the CAD data. The construction platform is lowered when the laser scanning is finished so that the laser beam can scan and deposit the next powder bed. Until all necessary parts are produced, the process is repeated for successive powder layers. The most important process variables in this technology are laser power, scanning speed, hatch spacing, and layer thickness (Figure 4).[62], [63] In the meantime, complex structures can be created by utilizing alternative scanning methodologies and process parameters for different areas of the component and supports. Furthermore, because a highly focused laser beam with a fast scanning speed is used, L-PBF is distinguished by quick cycles of heating, melting, solidification, and cooling. L-PBF samples that are subjected to extremely high cooling rates of up to 106 K/s develop a fine-grained structure and, eventually, improved mechanical properties. Conversely, L-PBF components with a high anisotropic microstructure, residual stress, and random porosity distribution are produced due to layer-by-layer fabrication and substantial temperature gradients.[64] Finer particles and less energy are needed to produce a fully dense component in the L-PBF process because of the pre-positioned powders on the substrate. Lower laser power and higher scan rates can be used to achieve this. [65] Because of its remarkable accuracy and precision, L-PBF is preferred for applications that demand complex geometries and superior surface quality. Its versatility is further increased by its ability to work with a variety of materials.[66]

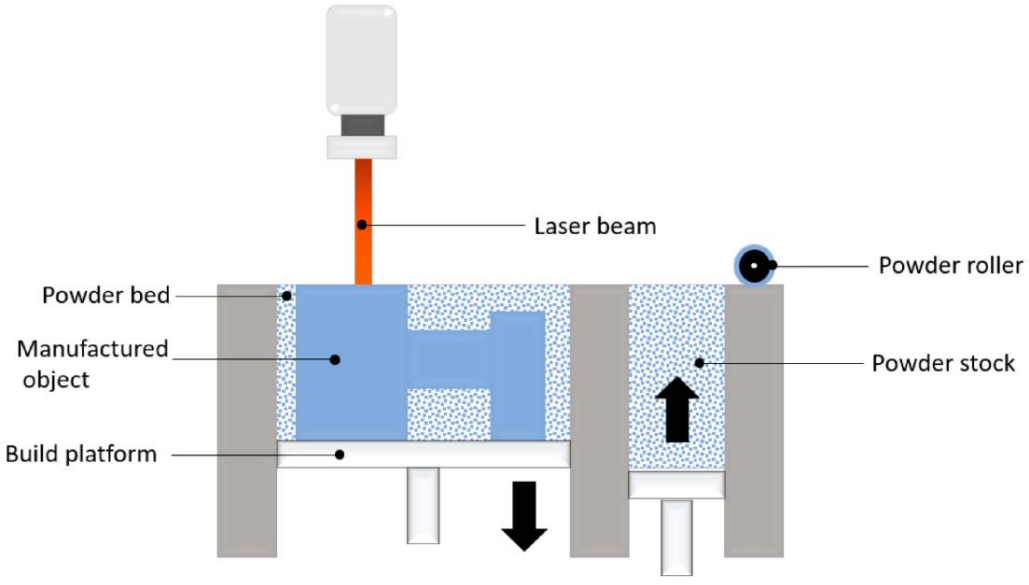

Figure 4 Schematic representation of L-PBF[67]

1.3.2.2.1 Surface characteristics of PBF components

Unlike components that are made traditionally, PBF components have distinct surface properties. The benefit of producing freeform geometries necessitates that the part be orientated with regard to the print bed at angles ranging from ±0 to 90°. Differently oriented parts have different asperities. The component's surface quality is impacted by these asperities. Additively manufactured items will inevitably have undesirable surface roughness and poor surface appearance, [68] as well as dimensional inaccuracy in micro-interior channels.[69] The components' surface roughness is influenced by the fusion processes, either melting or sintering [70]. The arithmetic mean deviation of the evaluated profile (Ra) ranges from 3 to 50 µm, whereas the average height of the evaluated profile (Rz) ranges from 20 to more than 150 µm, depending on the feedstock material [71]. A component's mechanical performance is more unpredictable when surface roughness varies widely.

When the component surfaces are used in lubrication, wear, and friction applications, their surface quality must be constant. A component's fatigue initiation life, endurance fatigue limit, and final separation life are all impacted by surface roughness. Higher surface roughness increases the likelihood of crack development and decreases fatigue life [72]. According to reports, AM components have a fatigue life that is 60% lower than that of conventionally machined components. Li et al. critically evaluated and compared the fatigue life of PBF and conventionally cast components; the as-built PBF components' fatigue life was never superior to that of the cast Ti-6Al-4V. Both (a) surface finish and (b) internal defects in PBF components significantly reduced the fatigue life.[73] Mower and Long examined Ti-6Al-4V's mechanical behavior and emphasized the importance of post-processing. Only 85% to 90% of the wrought materials' fatigue limit was reached by the as-built parts' maximum fatigue strength. The main causes of crack initiation were shown to be internal defects and surface roughness.[74] Similarly, according to Fousova et al., surface flaws were the primary cause of the crack start sites in PBF Ti-6Al-4V.[75] Surface irregularities have an impact on other mechanical characteristics, including surface hardness, corrosion resistance, and tensile strength, in addition to fatigue life.[[76], [77], [78] Aside from mechanical properties, the resulting dimensional integrity is poor. Particularly in microfeatures, high surface roughness results in dimensions that significantly exceed their tolerance limits [79]. In comparison to the design dimension, Hassanin et al. found that the horizontal (0°) build orientation had just 50%-dimensional integrity. The surface asperities, which range in size from 10 to 80% of the internal channel's diameter, were the cause of this [80]. Scans using X-ray computed tomography confirmed that Snyder et al. confirmed that dimensional non-conformance was caused by the ball-like asperities at the internal channel's down skin. This demonstrates how dimensional integrity is impacted by both surface quality and construction direction [81]. Furthermore, the circularity and concentricity of the microchannels are impacted by these asperities. Through numerical simulations, Solyaev, Rabinskiy, and Tokmakov established these findings regarding the over melting and shutting of thin horizontal channels [82]

The next section reviews the various asperity types present in PBF surfaces and how they affect surface roughness.

Types of surface defects

The main limitation of current metal PBF processes is poor surface quality, including texture, topology, and roughness, caused by loosely attached particles or defects. Laser-based PBF can achieve surface roughness (Ra) values as low as 5–10 μm, but in most applications, it still falls below the standard surface polish criterion of Ra < 1 μm. Despite using optimal process parameters for L-PBF, surface discontinuities can still be observed on additively manufactured parts. These discontinuities, which appear as loosely attached particles or partially sintered metal powders, can be attributed to the stair-stepping effect (SSE) inherent in the PBF process [83]. The AM construction approach requires that curvature and inclined surfaces be approximated in modest stages because it is layer-by-layer. SSE, therefore, plays a role in the greater surface roughness value and the more significant surface discontinuities. Metal powder particle size distribution, build orientations, and layer thickness are the primary variables influencing imperfections on AM components. Additional surface finishing is the last postprocessing step for any AM component created using the PBF process. Several surface finishing techniques are used to achieve the desired finishing effect for practical reasons. It is generally accepted that the following imperfections lead to high surface roughness:

(a) Loosely bonded powders: The raw powder material typically attaches to the surface of the component throughout the build process. During post-processing, a significant quantity of loosely bound powders trapped inside the channels present difficulties, as seen in Figure 5(a). Additionally, they contribute to significantly high surface roughness, and the loosely attached powder may be due to satellite powder [84]

(b) Partially melted powders: The high-temperature molten pool releases heat into the surrounding air during the laser melting process. Partial melting and solidification occur at the edges as a result of the surrounding powders being drawn to the melted edge by high thermal energy [85].

(c) Surface pores: As seen in Figure 5(b,c), low liquid front rates and fast scan speeds cause surface pores to form, which lowers the parts' densification. The molten pool significantly crumples and shrinks during the low liquid front, causing improper densification and pore development[86].

(d) Stair-casing: The down skin of parts constructed at orientations greater than 45° is typically where stair-casing defects, also referred to as the stair-stepping effect (SSE), are found. The primary cause of stair-casing is powder's high laser absorptivity, which leads to

the development of dross and spatter [87], [88]. As illustrated in Figure 5(b), it is also argued that increasing the layer thickness produces staircase effects.

(e) Balling melts: Balling melts are ellipsoidal or spherical objects that remain separate from the melted areas, as shown in Figure 5(c),(d). There have been reports of two different kinds of the balling phenomenon: (1) low laser power, which results in little liquid formation and a low degree of undercooling of the melt pool; and (2) high scan speeds, which cause metals to splash and cause balling melts on the surface [89], [90].

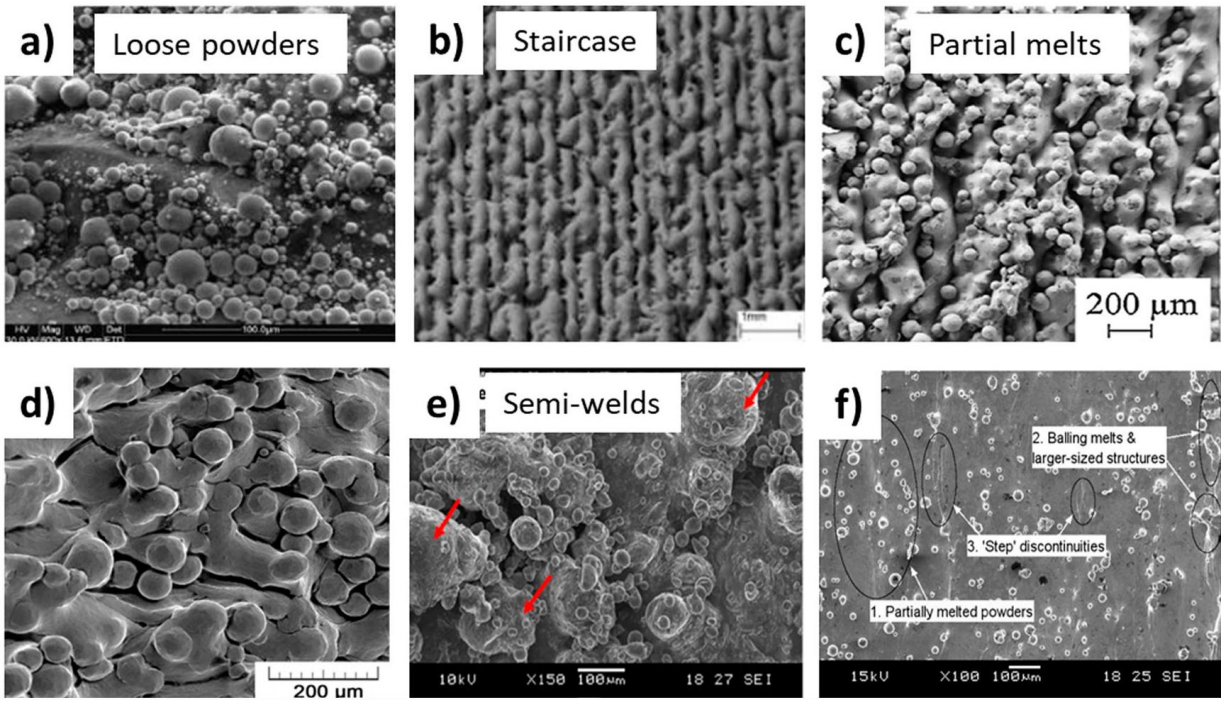

Figure 5 (a) Loose powders, (b) sintering layer steps, (c) partial melts, (d) balling effect, (e) semi-welded structures, and (f) balling melts and step discontinuities [91]

(f) Semi-welds: As seen in Figure 5(e), semi-welds are melted particles that are present on the surface and are comparable to the balling phenomenon. Half of these structures' surface appears to be partially welded. Clusters form of semi-welds are typically found [92].

(g) Step discontinuities: Another name for this phenomenon is a ripple front. As seen in Figure 5(f), high-temperature differentials between the molten pool and the traveling laser beam cause ripples to appear on the surface. The molten pool is sheared by a temperature gradient, and the high rate of solidification prevents the liquid metal from returning to its pre-solidification state, which causes step discontinuities and ripples. These show up as protuberances on the upper and lower surfaces [93], [94].

Controlling process parameters such as powder size, laser power, scan speed, oxygen content in the build chamber, laser overlap in the scan, layer thickness, part design, and other factors has helped eliminate some defects. However, this can only minimize others. In certain cases, the removal or reduction of surface defects can lead to part distortion and weakened mechanical strength. As a result, the inferior surface quality of as-built additive manufacturing (AM) components makes them less desirable for functional performance when compared to subtractive manufacturing processes.

A comprehensive review of the surface characteristics reveals the prevalence of various irregularities on powder bed fusion (PBF) components. Therefore, post-processing surface finishing of PBF components is essential before they can be deployed in practical applications. The next section will provide a thorough review of various surface finishing techniques that can enhance the surface quality of PBF components.

1.4 Surface post-processing for AM parts

Various surface post-treatments have been utilized for AM titanium alloy components to address the challenges associated with the inadequate surface quality of as-built parts material. In this section, Figure 6 illustrates how the treatments are categorized, primarily based on the inherent properties of the technology used and the resulting effects on the surface of the AM part. The main categories include “material removal," “no material removal," "coating," and a combination of treatments known as "hybrid treatments." The following section discusses each surface post-treatment in detail.

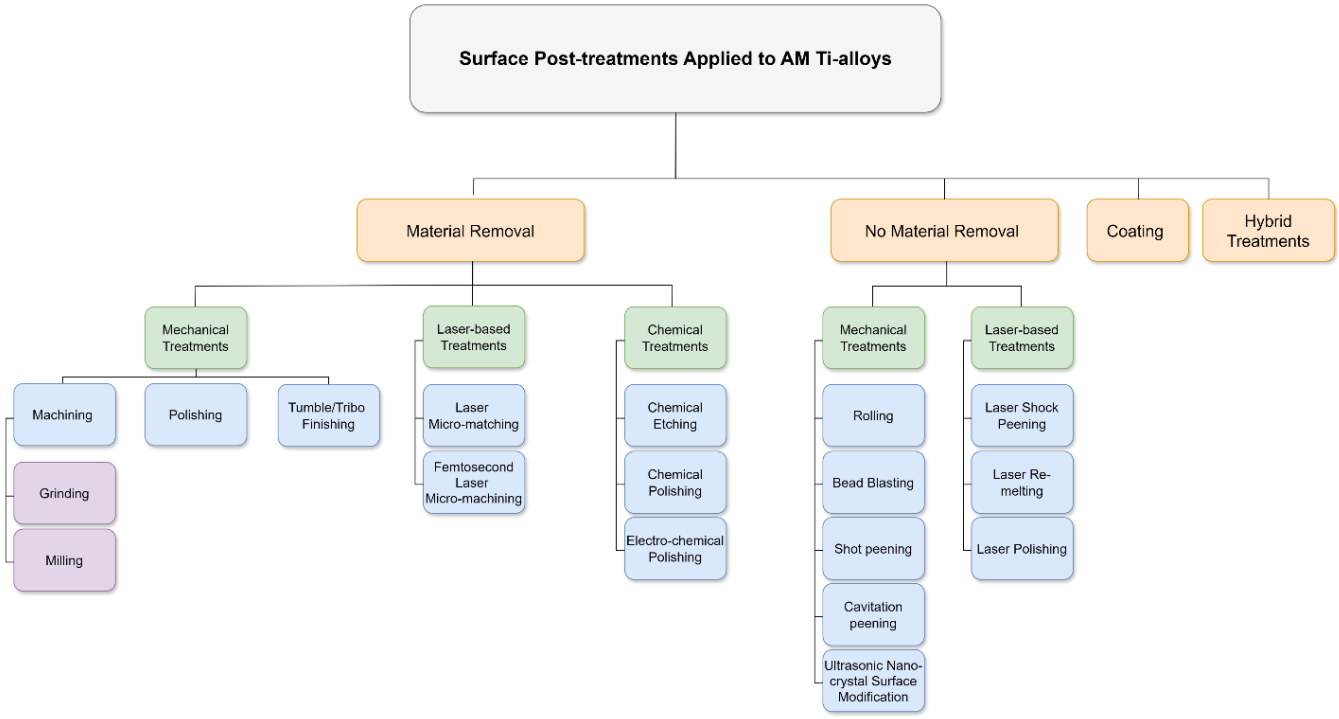

.

Figure 6 Categorization of the surface post-treatments applied to AM Ti-alloys, Adapted from[95]

1.4.1 Surface treatments based on material removal

This section discusses surface treatments that eliminate geometrical flaws on the top surface by removing a thin layer of material. The three primary categories into which these treatments fall—mechanical, laser-based, and chemical—are explained in the following subsections.

1.4.1.1 Mechanical treatments

1.4.1.1.1 Machining

Machining encompasses a range of technologies that use power-driven machines and cutting tools to remove material in controlled ways, forming objects with a smooth surface. It can be categorized into various procedures according to surface finish quality, cutting instruments, and motion.

The machining of titanium alloy components is challenging due to the material properties, moreover, the parts produced by AM technology are more susceptible to stick to cutting tool due to the layered wise structure which may result in delamination and defects [96]. However, there are numerous reports on the effect of machining on the enhancement of surface characteristics of additively manufactured titanium parts. After machining, the as-built LPBF Ti-6Al-4V samples'

surface roughness, which represented an arithmetic mean (R/), was significantly decreased to 0.89 µm and bending fatigue strength improved by 30% [97]. Another work reported a minimum surface roughness achievement 19.21 nm by micromachining of Ti-6Al-4V L-PBF fabricated parts [98]. Few other mechanical material removal techniques can be classified as machining, which have been employed to improve the surface quality of AM metallic parts. These include grinding [99], and milling [100]. Figure 7 depicts the effects of grinding on the roughness of Ti-64 AM parts.

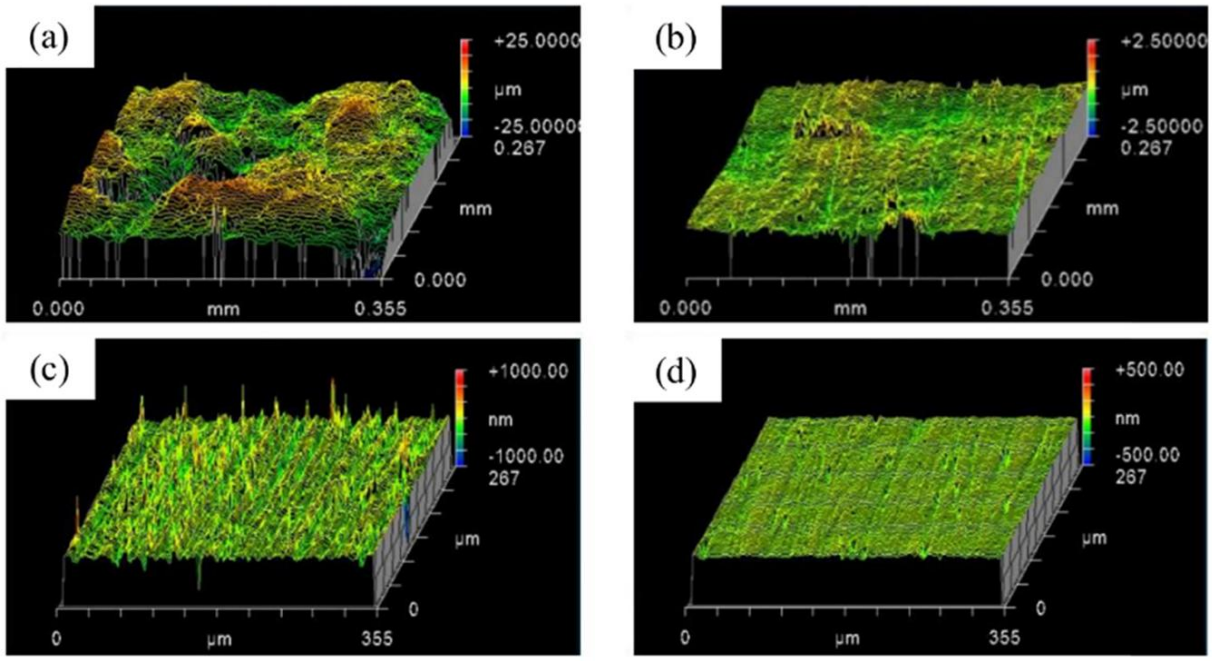

Figure 7 Surface topography of PBF Ti–6Al–4V (a) before grinding with Ra=4.13 µm; after grinding using different grinders including (b) 40 µm Nickel bonded grinder leading to R a =130.8 nm, (c) 9 µm Nickel bonded-grinder with Ra =65.6 nm and (d) 3 µm Resin bonded-grinder with R a of 17.9 µm adopted from [99].

1.4.1.1.2 Polishing

Polishing is the process of achieving a mirror-like finish on a workpiece's surface. Many studies have reported the use of mechanical polishing to enhance the surface quality of additive manufacturing (AM) metallic materials, specifically aiming to improve their fatigue behavior [101], [102]. The EB-PBF based additive manufactured Ti-6AL-4V results show that the subsurface maximum principal residual stresses decreased by 108%, the average surface roughness decreased by 33% [103]

1.4.1.1.3 Tumble finishing

Tumble finishing (TF) or barrel finishing is a mass surface finish improvement process where parts, media, and compounds are placed in a rotating barrel to reduce roughness, controlled by parameters such as abrasive material size and the barrel's rotation speed. Applying TF to LPBF Ti–6Al–4V samples resulted in a minor decrease in surface roughness in terms of Sa (from 21.5 to 18.9 µm), which improved fatigue life significantly [104]. Application of the tribo-finishing process to the L-PBF Ti–6Al–4V ELI part, as illustrated in Figure 8, resulted in a surface roughness reduction from 6.83 µm in terms of Ra for the as-built samples to 4.96 µm after tribo-finishing. Consequently, the fatigue limit of the treated material increased up to about 40% [105]. This approach eliminates the highest peaks without necessarily affecting the deeper valleys on the surface, as shown in Figure 8.

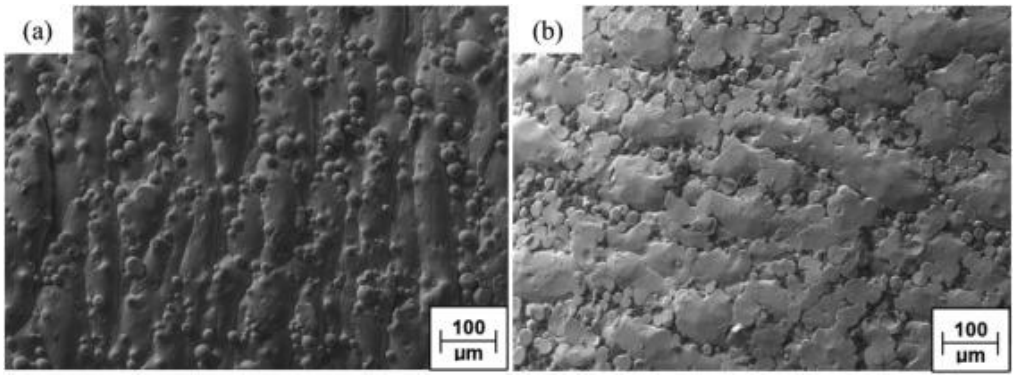

Figure 8 SEM micrographs showing the LPBF Ti–6Al–4V ELI samples' surface morphology: (a) as constructed, and (b) following tribo-finishing adopted from [105].

Vibratory grinding, a very comparable mechanical surface treatment, was also reported to reduce the as-built LPBF Ti–6Al–4V samples' surface roughness in terms of R a from 17.9 to 0.9 µm [106]. In AM combined with TF, surface roughness reduction is shaped by the accessibility of media to partially melted powder and initial ridge heights on surfaces. The initial average roughness (Sa) is ranked as: down-skin (most rough), side-skin, and up-skin (smoothest). The rate of Sa reduction follows this order: side-skin, up-skin, and down-skin. This behavior is linked to the initial entrapment of partially melted powder and ridge heights, which were influenced by the surface build orientation during AM, leading to variations in initial surface peak material volumes.[107]

1.4.1.2 Laser-based treatments

This section discusses the use of laser surface treatments to enhance the quality of additive manufacturing metallic parts by removing material. Laser micro-machining is a widely used

surface treatment technique that utilizes various wavelengths, waveforms, and pulse durations. In the femtosecond laser micromachining process, the laser beam is focused on the material's surface. Dielectric mirrors are specifically designed to reflect the optimal laser wavelength, minimizing energy loss during this process [108]. The application of femtosecond laser micro-machining to LPBF Ti–6Al–4V parts significantly decreased the surface roughness in terms of Ra from 4.22 μm to 0.82 μm for the as-built and treated material, respectively [109].

1.4.1.3 Chemical Treatments

Another popular class of methods for reducing the unwanted surface roughness of AM metallic materials as-built is chemical treatment. Chemical surface treatments are primarily used for parts and components with complex geometries, such as lattice and cellular structures, because they can be applied globally to all of a part's surfaces and, in contrast to mechanical treatments, provide access to the complex internal surfaces. Chemical treatments are also frequently used in metallic AM components to improve the surface finish quality locally after support structures are removed. [110]. The primary techniques in this area are as follows: chemical etching [111], [112], [113], chemical machining [114], chemical brightening, and chemical polishing [115]; also electrochemical polishing (ECP) [116]. Some representative images of each of the above-mentioned techniques are displayed in Figure 9. With only minor variations in length or operating temperature that directly impact the depth of material removal, these chemical treatments are all based on immersing the AM component in temperature-regulated baths of chemical solutions. For instance, in chemical brightening, the settings are adjusted to produce a shiny metallic surface and a mirror-like finish.

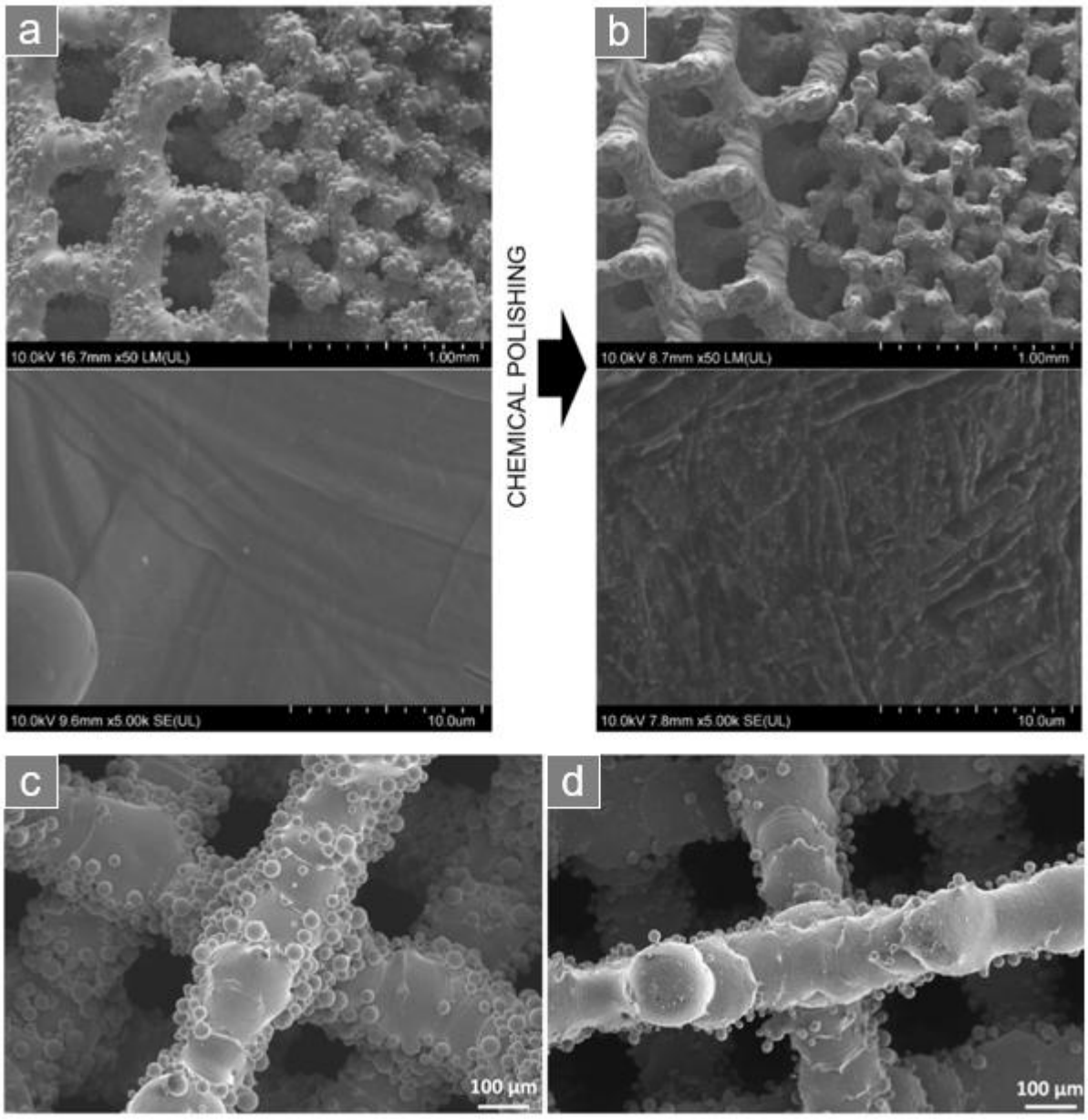

Figure 9 Overall view of titanium scaffolds and texture of their surface before (a) and after (b) chemical polishing. Surface of the struts at higher magnification is depicted in the lower images[115]. Surface morphology of the SLM processed lattice Ti6Al4V samp

Furthermore, a few additional chemical treatments are given to AM metallic materials with the intention of inducing particular surface features to adjust the surface properties according to the final application, rather than particularly lowering the surface roughness. The acid-alkali (AcAl) treatment that is frequently applied to Ti–6Al–4V components in order to further bio-functionalize them is a typical example [117]. By altering the surface chemistry of the structure and producing nano-features, these treatments are employed to bio-functionalize the surface.

1.4.2 Surface treatments based on no material removal

Applied surface post-treatments enhance the surface and mechanical properties of additive-manufactured metallic parts through plastic deformation without material removal. This deformation is achieved by applying loads or impacts and transferring kinetic or thermal energy, affecting either just the surface or also the bulk material. These treatments are categorized into mechanical and laser-based technologies, as detailed in the following sections.

1.4.2.1 Mechanical treatments

1.4.2.1.1 Rolling

Rolling deforms the surface of AM parts using rollers to reduce thickness or smooth the surface. Mainly applied in WAAM and sometimes in liquid metal deposition [[118],[119], it can enhance surface finish, induce compressive residual stresses, and refine grains if optimized [120],[121]. Strategies include single-pass or inter-pass rolling during deposition [122].

1.4.2.2 Sand/Bead Blasting (SB)

SB uses abrasive particles (e.g., sand, ceramic beads) to reduce surface roughness and clean surfaces. It has shown effectiveness in LPBF AlSi10Mg, 316L, and Ti–6Al–4V by lowering roughness and inducing compressive stresses [123],[124], [125]]. SB improved fatigue performance better than vibratory grinding or micromachining [126], [127], and is widely used in biomedical applications to improve surface quality [128], [129]].

1.4.2.3 Shot Peening (SP*)*

SP bombards the surface with small shots to introduce compressive residual stress and improve fatigue life [[8], [13], [14], [15]]. Applied to LPBF metals, SP enhances hardness and grain refinement but doesn't fully smoothen the surface. It outperforms TF and ECP in fatigue strength improvement, shifting crack initiation below the surface due to higher compressive stresses (Fig. 12) [[130], [133]].

1.4.2.4 Cavitation Peening (CP)

CP uses collapsing bubbles (not solid shots) to induce surface stress and reduce roughness. Applied to PBF Ti–6Al–4V, CP slightly improved roughness and fatigue performance, though SP remained more effective overall [[17], [18]]. A combined technique using abrasive water cavitation further improved roughness and fatigue strength (up to 66%) [136].

1.4.2.5 Ultrasonic Nano-Crystal Surface Modification (UNSM)

UNSM applies ultrasonic-frequency impacts with a WC tip to refine surface grains, increase hardness, and induce compressive stresses [[137], [138]]. Applied to LPBF NiTi, Ti–6Al–4V, 316L, and DED AISI M4, UNSM effectively reduced roughness, enhanced corrosion and wear resistance, and improved mechanical strength, though it reduced elongation in some cases [138], [139]].

1.4.3 Laser-based treatments

A laser beam is pulsed on the surface of a metallic target material during laser shock peening (LSP), creating shock waves that are caused by laser ablation of a sacrificial layer (or water) on the sample's surface. These shock waves propagate throughout the material's surface layer, causing plastic deformation and adding compressive residual stresses.

1.4.3.1.1 Laser shock peening

When a metallic target material is subjected to laser shock peening (LSP), a laser beam pulses onto its surface, creating shock waves that are caused by laser ablation of a sacrificial layer (or water) on the sample's surface. These shock waves propagate throughout the material's surface layer, causing plastic deformation and compressive residual stresses[140]. The effects of LSP have been examined and compared on mechanical properties and fatigue behavior of PBF Ti–6Al–4V samples [134].

1.4.3.1.2 Laser re-melting

Prior to the deposition of a new layer, the residue partially connected powders are melted by a second laser source passing on the deposited layer, a process known as laser re-melting. In this instance, many approaches have been used: either re-melting all of the layers during manufacturing, which might significantly lengthen the production time, or re-melting only after the final outer layer of the geometry has been fabricated. The purpose of this approach has been to decrease porosity and roughness [141], [142]. Increased current, reduced scanning speed, and higher overlaps have been reported to result in improved performance of the laser re-melting process [[143], [144]].

1.4.3.1.3 Laser polishing

Reducing the surface roughness of AM parts without causing ablation is possible via laser polishing, which is conceptually very similar to laser re-melting. The laser uses low laser pulses with a power density that can produce local surface melting of a few nanometers to micrometers

to irradiate the material's top surface in this process [145]. Figure 10a and b illustrate the difference between the surface roughness of PBF Ti–6Al–4V parts in as-built configuration and after laser polishing [146]. In addition effects of laser polishing on surface roughness reduction and fatigue behavior improvement of LPBF Ti–6Al–4V parts were inspected [147]. The results indicated remarkable surface roughness decreasing from 14.21 µm in terms of Sa (as-built) to about 1.77 µm after laser polishing.

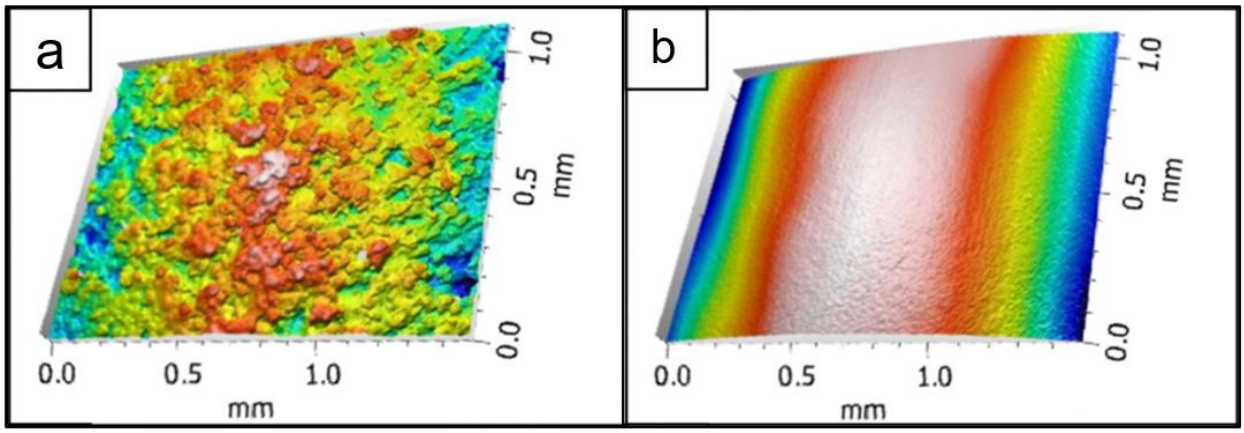

Figure 10 Surface topography of L-PBF Ti-6Al-4V for (a) as-built and, (b) laser polished specimens. Note that images are not curvature corrected[148]

1.4.4 Coating

Coating is regarded as a useful method for controlling the surface properties of AM materials or adding additional surface functionality. Coatings have been used to improve surface quality, conceal flaws, and reduce roughness. Coatings are also used to adjust the AM parts' resistance to corrosion or tribology. In other instances, coatings are used to provide regulated surface morphologies that improve the AM metallic materials' biological performance [149], [150].

Hydroxyapatite coating was applied to lattice structures of laser powder bed fused (LPBF) Ti–6Al–4V by immersion in simulated body fluid (SBF) for up to three weeks, significantly reducing surface roughness and enhancing bioactivity through the formation of bone-like apatite layers [134,135]. Other surface modification techniques, such as silver-impregnated chitosan coatings via electrophoretic deposition [151], and anodizing to create Titania nanotube arrays [152], [153], have been widely used on AM Ti-based materials to improve mechanical properties, corrosion resistance, and biological performance. Plasma electrolytic oxidation (PEO), a technique derived from anodization, has also been applied to porous LPBF Ti–6Al–4V implants to address implant-associated infections by forming micro/nano-porous Ti oxide layers with strong antibacterial effects and enhanced cytocompatibility[154], [155]. These surface treatments collectively improve

hydrophilicity, osseointegration, and cell adhesion, while maintaining or modestly enhancing mechanical integrity, wear resistance, and other functional properties of the AM metallic structure

1.4.5 Hybrid treatments

Hybrid post-treatment methods have appeared to address regular problems in additive manufacturing of titanium alloys, such as surface roughness, residual stresses, and internal porosities. These methods combine thermal, mechanical, and chemical processes to enhance structural integrity and surface properties of AM-produced titanium components[156][157]; Accordingly, multiple studies have underlined the benefits of combining surface finishing techniques with thermal treatments to improve the fatigue strength of additively manufactured components. Since mechanical procedures such as milling, turning, grinding, and machine polishing are effective in reducing surface roughness and improving fatigue performance, their utility is sometimes limited caused by internal porosities and lack-of-fusion defects integral to AM processes[158], [159].

Therefore, to modify the surface or bulk properties of additively manufactured metallic materials to meet the functional requirements of specific applications, it is conventional practice to use a combination of two or more post treatment methods. Among these, the integration of heat treatment (HT) with surface modification techniques has been proved as one of the most avant-garde hybrid methods[160]. HT is normally applied to homogenize the microstructure, reduce anisotropy, and recover undesirable tensile residual stresses in AM metals[161]. Further commonly implemented thermal post-treatment is hot isostatic pressing (HIP), which simultaneously studies the component in raised temperatures and isostatic gas pressure[162]. In supplement to its microstructural refinement capacities, HIP has demonstrated very effective in reducing internal porosities, unless those voids are greatly interconnected or located near the surface[163]. The elimination of unmelted material is also eased by the induced plastic flow and minimal material transfer developing under the low-pressure environment of HIP[164].

In a study led by Dohoon Lee and colleagues[165], the impacts of annealing and Hot Isostatic Pressing (HIP) on the microstructure and mechanical performance of selective laser melted (SLM) Ti–6Al–4V alloy were examined. The results showed that the high cooling rates naturally related to the SLM process result in a columnar prior-β grain structure filled with acicular α′ martensite in the as-built situation. Annealing at 735°C accelerated the transformation of this metastable α′ phase into a mixture of α and β phases, increasing the β-phase fraction whilst maintaining the original morphology and HIP at 930°C enabled substantial coarsening and spheroidization of the α and β phases, resulting in clear grain growth and a more thermally stable, equiaxed microstructure. Both post-processing treatments also contributed to the reduction of residual stress, as evidenced by mapping, with HIP demonstrating greater stress relief due to the high processing temperature[165].

As proved in another study[166], Ti-6Al-4V samples manufactured by AM that undergo surface polishing followed by HIP exhibit fatigue limits approaching the theoretical upper bound(1.6HV ± 0.1HV) but as-built cases achieved only about 27% of the ideal fatigue limit predicted from Vickers hardness measurements so this difference clearly shows that the combined application of surface polishing and HIP due to the reduction in surface defects and internal porosity, could be deemed as very effective at improving the fatigue properties of additively manufactured materials.

According to findings by a study [167], the results of hybrid surface treatments on Ti-6Al-4V alloy produced via hot isostatic pressing, with elaboration on the combined application of heat treatment and ultrasonic surface rolling process (USRP); As outcome, a heating-assisted ultrasonic surface strengthening (HUSS) technique, performed at 150 °C, was led to improve surface properties by integrating thermal softening with mechanical deformation. The heat-treated sample under USRP showed a grain size of ~200 nm, increased microhardness and surface roughness and despite the higher hardness, these samples exposed significant wear rates due to less beneficial microstructural variations.

Subsequent to these thermal procedures, mechanical and chemical surface treatments such as shot peening and electropolishing have shown considerable ability in improving surface integrity. Shot peening (SP) which is commonly identified as one of the greatest efficient procedures for modifying the surface layer of metallic materials[168]. Electropolishing (EP) is also an effective electrochemical method for polishing metal surfaces by presenting a smooth and clean finish without compromising the structural integrity of the component while also improving corrosion resistance[169]. Integrating shot peening (SP) and electropolishing (EP) as sequential post-processing treatments for additively manufactured (AM) titanium alloys, bears considerable prospective for improving material performance[170] while also as shown in a research conducted by M. Kiel and their colleagues [171]has explored this hybrid treatment approach on additively manufactured Ti–6Al–4V alloys(with DED and PBF) as their findings indicate that using electropolishing after shot peening alleviates surface roughness and removes trapped shot particles and the hybrid post treatment has demonstrated increases in corrosion behavior.

A hybrid post treatment strategy as used for examining the fatigue behavior of PBF additive manufactured TI6AL4V alloy[172], used the subsequent application of shot peening followed by a surface enhancement process known as CASE, which falls under the category of chemically assisted tumbling techniques, functioning similarly to the extreme isotropic superfinishing (ISF) process [173][174]. The main aim of the CASE treatment is to reduce the surface roughness introduced by shot peening, in this way reaching a smoother finish while maintaining the beneficial compressive residual stresses instructed by the initial peening stage. As also observed in another research, specimens treated with shot peening+CASE demonstrated a smoother surface finish, which contributed to improved fatigue life, with all crack initiation sites located in the interior of the material [175]

2 Materials & Methods

2.1 Samples Manufacturing

The Ti-6242 samples were manufactured using L-PBF technology. Prior to producing the samples designated for surface post-treatment, printing parameter optimization was carried out to enhance both the bulk and surface quality. This step was essential, as printing parameters can significantly influence surface characteristics.

2.1.1 Parameter optimization

2.1.1.1 Design of Experiment

The Design of Experiment (DoE) encompasses one of the key factor considered in the parameter optimization L-PBF multiple adjustable parameters influence the manufacturing process. Among the most influential parameters are layer thickness, laser power, spot size, scanning speed, and hatching distance. To evaluate different parameter combinations, Volumetric Energy Density (VED) was introduced in previous studies. The VED is calculated as:

$$VED = \frac{P}{v \cdot h \cdot l}$$

Where:

- VED = Volumetric Energy Density [J/mm3][$J/mm3$]
- P = Laser Power [W][W]
- v = Scanning Speed [mm/s][mm/s]
- h = Hatching Distance [mm][mm]
- l = Layer Thickness [mm][mm]

The VED represents the energy applied per cubic millimeter of powder, serving as a key metric for process optimization. In this study, in order to optimize the manufacturing parameter, based on previous studies narrow range of parameter, as three level for laser power [180,200,220 W] and three level for laser scan speed [1000,1200,1400] is considered and other parameters remain constant. Table 2 lists the calculated VED values and corresponding parameters input.

Table 2 Printing parameters for Ti-6242

Sample number	Laser Power (W)	Scanning speed (mm/s)	Hatch distance (mm)	Layer thickness (mm)	VED (J/mm³)
1	180	1000	0.08	0.03	75.0
2	180	1200	0.08	0.03	62.5
3	180	1400	0.08	0.03	53.6
4	200	1000	0.08	0.03	83.3
5	200	1200	0.08	0.03	69.4
6	200	1400	0.08	0.03	59.5
7	220	1000	0.08	0.03	91.7
8	220	1200	0.08	0.03	76.4
9	220	1400	0.08	0.03	65.5

2.1.1.2 DoE sample preparation

A gas-atomized Ti–6Al–2Sn–4Zr–2Mo powder with a particle size ranging from 15 µm to 55 µm and an average diameter of 32 µm was used as the starting material. Cubic samples of $8 \times 8 \times 10$ mm^3 (L × W × H) were fabricated using a Print Sharp 250 machine, Figure 11. Before the commencement of the fabrication process, an argon gas environment was introduced into the chamber to maintain the oxygen content below 0.2%, thereby toning down the potential impact of oxygen on the fabrication process.

Figure 11 Prima Additive Print Sharp 250 machine

The workflow began with job file preparation shown in Figure 12, by using Materialise Magics, a software tool commonly used for preparing and optimizing additive manufacturing (AM) designs. This stage involved support generation (if needed), part orientation, and slicing, resulting in an output file in .CLI format. The .CLI file was then imported into EPhatch, a software designed for assigning critical process parameters, including laser power, scan speed, hatch spacing, and exposure time. These parameters significantly influenced part density, microstructure, and mechanical strength. The parameters used for this project are instructed in Table 2. After defining the settings, the data was converted into .EPI format, making it compatible with the Print Sharp 250 machine.

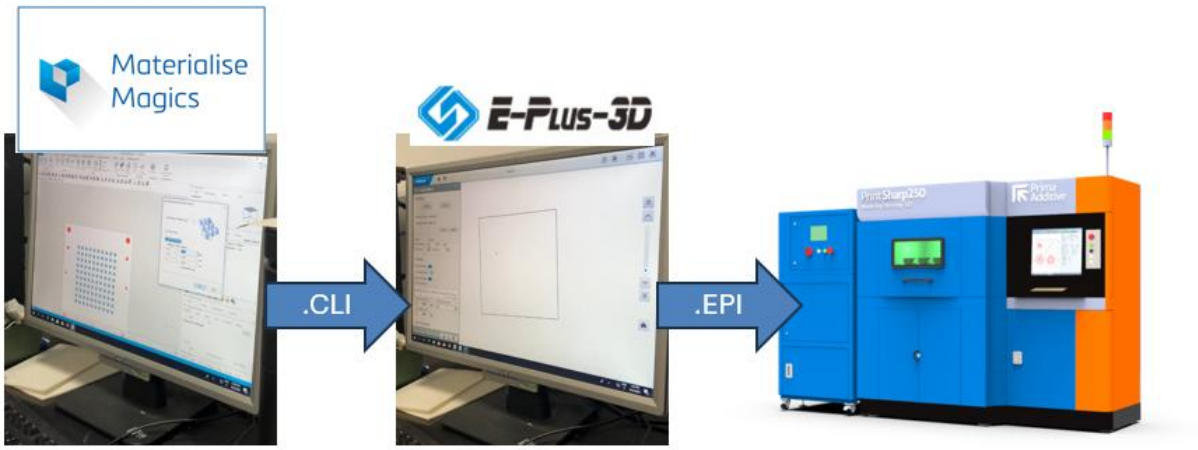

Figure 12 Print Sharp 250 machine job file preparation flow.

Prior to initiating the printing process, the machine was prepared by an operator. The preparation involved filling the powder bed with Ti-6242 metal powder and ensuring a controlled atmosphere within the build chamber by using argon gas flow to reduce oxidation risks. The initial layers of the build were particularly critical, as any instability in the laser-material interaction could lead to defects such as porosity, lack of fusion, or warping. Therefore, it was crucial to monitor these initial layers closely to ensure a stable and uniform build process.

Upon completion of the print job, the parts were allowed to cool inside the chamber to prevent thermal stresses and cracking. Once cooled, the build platform was ejected from the machine by the technician, marking the beginning of the post-processing phase.

2.1.2 WEDM

Wire electrical discharge machining (WEDM) is a non-conventional machining process that uses electrical sparks to erode conductive materials, producing complex shapes with high accuracy and good surface finish. Key performance measures include material removal rate, surface roughness, and kerf width.[176] WEDM can machine a wide range of conductive materials regardless of hardness, making it suitable for advanced engineering materials like superalloys and composites.[177] The e.cut WEDM machine was employed to cut the samples at this step. This machine is shown in Figure 13, the main part of the machine is where the workpiece is placed for the cutting operation. Initially, the platform was secured to the wire-cutting machine using clamps. Next, in the software used for positioning the wire in the machine, the wire was set on the platform to establish the reference points for both the x and y coordinates. After that, the wire's position was adjusted according to the platform's settings, and the correct dimensions and orientation were loaded into the machine to begin the cutting operation.

Figure 13 WEDM machine configuration during cutting

2.1.3 Characterization of optimal parameters

Following detachment, the printed components, which are depicted in Figure 14 underwent characterization to assess porosity and surface quality. This evaluation process included optical microscopy analysis, density measurements, and computed tomography (CT) scans to detect internal defects. These characterization techniques provided valuable insights into the effectiveness of the optimized parameters, guiding further refinement in L-PBF process settings.

Figure 14 L-PBF Ti-6242 test samples

2.1.3.1 Stereomicroscope

Stereomicroscopy provides three-dimensional visualization of specimens at relatively low magnifications. Unlike compound microscopes, stereomicroscopes utilize two separate optical paths to deliver slightly different perspectives to each eye, resulting in a stereoscopic effect that enhances depth perception. This feature is particularly beneficial in additive manufacturing (AM) for inspecting and characterizing the surface morphology of printed components. In the context of AM, stereomicroscopy serves as a valuable tool for the non-destructive examination of surface features, enabling the detection of defects such as cracks, porosity, and partially melted powder. Integrating stereomicroscopy into the AM workflow enhances the ability to identify and address issues early in the production process, thereby improving overall manufacturing efficiency and product reliability.[178], [179] Figure 5 demonstrates the detection of the surface quality of additively manufactured samples with a stereomicroscope image.

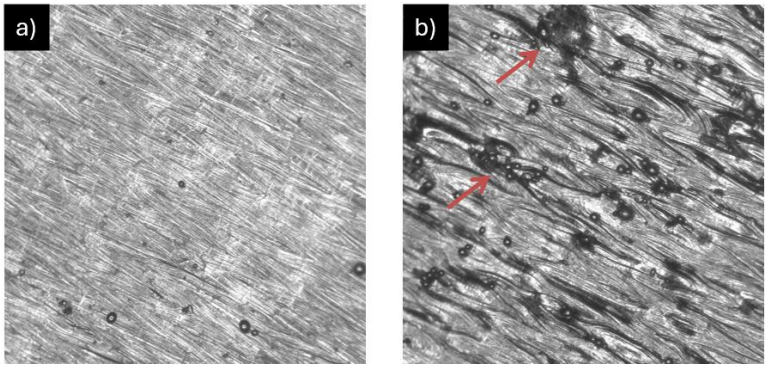

Figure 15 stereomicroscope image of upper surface a) sample 4 [P=200 W, V=1000 mm/s , VED= 83.3 [J/〖mm〗^3]] b)sample 3 [P=180 W, V=1400 mm/s, VED= 53.6 [J/〖mm〗^3]

2.1.3.2 Density Measurement

The Archimedes method is widely used for measuring density in laser powder bed fusion (LPBF) parts, offering a cost-effective and easy-to-use approach. [180] Archimedes' technique involved balancing geometric shapes using centroids and the principle of the lever to determine volume ratios. [181] According to ASTM F3637-23 [182], the Archimedes density measuring method makes it possible to calculate total porosity.

$$\rho_{\text{Archimedes}} = \rho_{\text{liquid}} \times \frac{w_{\text{dry}}}{w_{\text{dry}} - w_{\text{wet}}} \quad (1)$$

$$\rho_{\text{Geometrical}} = \rho_{\text{liquid}} \times \frac{w_{\text{dry}}}{w_{\text{wet}} - w_{\text{immersion}}} \quad (2)$$

$$\text{Total porosity percentage} = \frac{\rho_{\text{theoretical}} - \rho_{\text{bulk}}}{\rho_{\text{theoretical}}} \times 100\backslash\% \quad (3)$$

$$\text{Relative Archimedes Density percentage} = \frac{\rho_{\text{Archimedes}}}{\rho_{\text{theoretical}}} \times 100\backslash\% \quad (4)$$

Where:

$$\rho_{\text{Archimedes}} = \text{Archimedes density (apparent density)} \left[\frac{g}{cm^3}\right]$$

$$\rho_{\text{Geometrical}} = \text{Geometrical density (bulk density)} \left[\frac{g}{cm^3}\right]$$

2.1.3.3 X-ray computed tomography

(CT) is a non-invasive imaging technique that produces three-dimensional images of an object's internal structure. It utilizes X-rays and a rotating source-detector system to acquire multiple projections, which are then mathematically reconstructed into a 3D image. CT offers improved contrast compared to conventional radiographs, albeit with reduced spatial resolution. The technique finds applications across various fields, including medical diagnostics, materials science, engineering, and paleontology. [183], [184] One such advanced system used for CT analysis is the Phoenix v|tome|x s, a versatile high-resolution system designed for both 2D X-ray inspection and 3D computed tomography, including micro-CT and nano-CT imaging. The system offers high flexibility as it can be equipped with either a 180 kV/15 W high-power nano focus X-ray tube or a 240 kV/320 W microfocus tube, enabling a broad range of applications. Due to this unique combination, the v|tome|x s provides extreme high-resolution scans for low-absorbing materials while also allowing 3D analysis of high-absorbing objects.[185] These capabilities make it an effective and reliable tool for evaluating AM components, detecting unmelted powder regions, voids, cracks, and structural inconsistencies.

Figure 16 Phoenix v|tome|x s CT machine with integrated interface

To ensure that the sample remained inside the X-ray imaging frame, its position was checked and adjusted using the device's associated software, as seen in Figure 16. The tomography procedure started as soon as the proper positioning was established. It is essential to uniformly reset the detector with X-rays in order to remove any leftover residue before adding another specimen for tomography.

For the analysis and visualization of CT data, VGSTUDIO MAX software is used, the software environment is shown in Figure 17. This advanced software allows for high-precision 3D reconstruction, porosity analysis, defect detection, and dimensional measurements of AM components. With its powerful image-processing tools, the software enables detailed assessment of internal structures, helping to ensure the quality and reliability of 3D-printed parts.

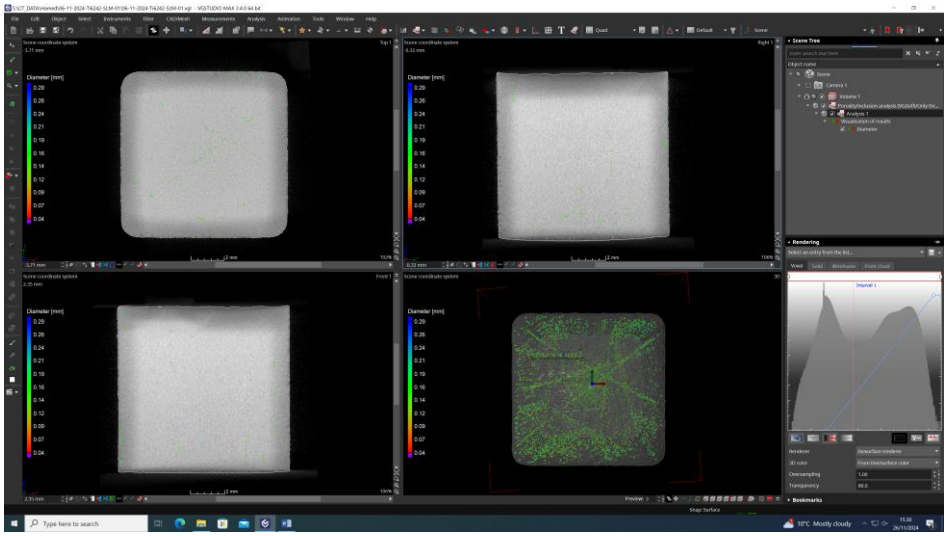

Figure 17 VGSTUDIO MAX software environment

2.1.3.4 Surface Roughness measurement

To describe the surface texture of the pieces produced, a profilometer (RTP80-TL90, Someco SM SRL, Italy) was used to assess surface roughness, as shown in Figure 18. In order to identify height variations and provide a complete profile of the surface topography, the apparatus moves a high-precision stylus across the surface. Important roughness metrics that provide an indication of the sample's surface integrity and manufacturing quality, such as Ra (arithmetical mean roughness), Rz (profile height, maximum), and Rt (total height variation), can be measured using this method. Three distinct measurements were made on each sample at various locations to guarantee accuracy and dependability. To minimize localized fluctuations and measurement uncertainties, the typical roughness parameter for each surface was calculated by averaging the acquired values. Using normal surface metrology principles, the profilometer was set up with the proper cut-off lengths and stylus speed settings. Surface roughness measurements and mechanical analyses can be used to provide a comprehensive picture of material performance and optimize process parameters for improved surface quality.

Figure 18 Profilometer RTP80-TL90

2.1.4 Surface post processing

In order to reduce the roughness and improve the surface quality the surface post processing has been done Figure 19, presented the summary of post-treatments techniques has been opt in this study.

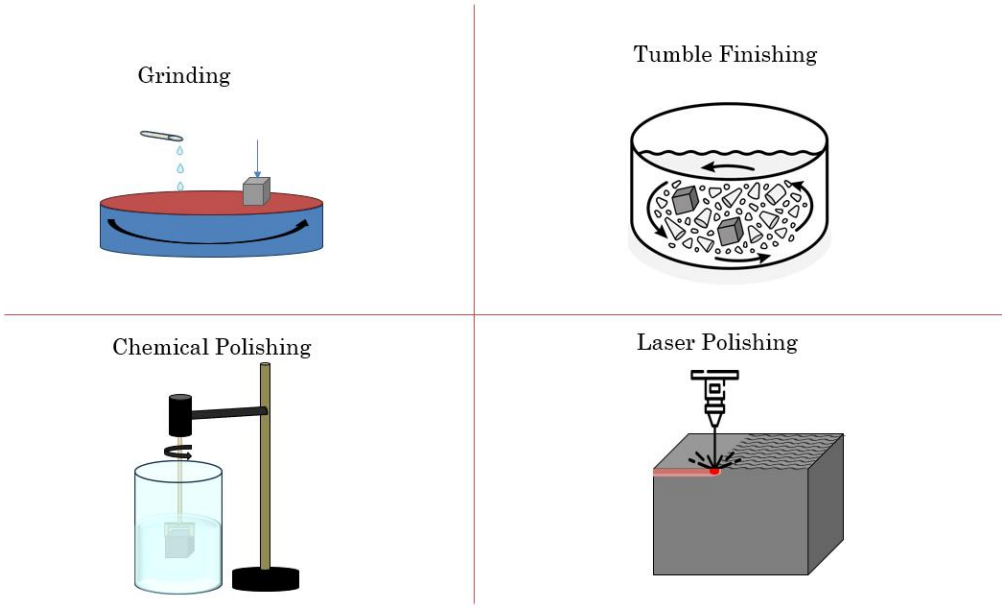

Figure 19 schematic of the surface post-treatments

Grinding

Manual surface grinding was conducted utilizing Presi Minitech 250/300 SP1 grinding machine, Figure 20, under continuous running water to prevent overheating and material contamination, as demonstrated in Figure 19. Silicon carbide abrasive paper with progressively finer grit sizes, concluding with P1200, was utilized to achieve a uniform surface finish.

Figure 20 Presi Minitech 250/300 SP1 grinding machine

Tumble Finishing

Wet tumble finishing has been done using Silco centrifugal disc finishing machine – 50 litre sifter capacity, Figure 21, for 3 hours, with 200 rpm rotation speed with ceramic cone as abrasive media. The samples has been paced in the barrel and the machined set for determined time and rotation speed.

Figure 21 Silco centrifugal disc finishing machine and ceramic abrasive media

Chemical Polishing

Chemical polishing was conducted by placing the specimen in 50 mL of an etchant containing 94ml distilled water+ 1.5 ml hydrochloric acid+ 4 ml nitric acid, a ratio similar to what is found in the literature for titanium alloys [186]. A conventional magnetic stirrer have been us during chemical polishing process to avoid saturation gradient. The experimental setup is presented in Figure 19. The samples have been placed in stirred media for 30 minutes in media, and then immediately washed with distilled water and dried.

Laser Polishing

Using a Concept-Laser Mlab-cusing-R system equipped with a 100 W fiber laser and a beam size of 50 µm the laser polishing has been done on the surface of sample with the laser parameter reported in Table 3.

Table 3 Laser polishing parameters

Setting	Laser Power [W]	Laser Scan Speed [mm/s]	Hatch distance [mm]	Layer thickness [mm]	VED [J/mm^3]
Laser Polishing	40	700	0.03	0.03	63.5

2.2 Characterization

2.2.1 Metallography

After completing surface post-treatments, specimens were cut using WEDM to expose the cross-section for metallography and nanoindentation. Samples were mounted using a 2:1 mixture of acrylic resin (KMU) and methyl methacrylate hardener. The mixture was poured into molds and cured for 15 minutes before being removed and prepared for grinding and polishing. Grinding was performed using a Presi machine, Figure 20, with abrasive papers of P480, P600, P800 ,and P1200 grit. Each sample was ground starting with the coarsest paper, using water for lubrication, cooling and debris removal. After each stage, samples were inspected under a microscope; if grinding lines were visible, the sample was rotated 90° and a finer grit was used. Polishing followed to remove scratches from grinding. Pads with 3 µm and 1 µm diamond suspensions were used, followed by a final polish with a 0.3 µm aluminum oxide solution to achieve a smooth, mirror-like finish. Prepared samples were then etched with 100 mL of Kalling's No. 2 solution for 20 seconds, rinsed, and dried. Finally, the microstructure and treatment depth were examined under an optical microscope.

2.2.2 SEM analysis

Surface morphology of the samples was characterized using SEM. Prior to imaging, samples were ejected from the mount. SEM imaging was performed using a JEOL JCM-6000Plus, Figure 22, operated at an accelerating voltage of 5 kV. Micrographs were obtained at various magnifications to assess surface features.

Figure 22 Versatile Benchtop SEM JEOL JCM-6000Plus

The analysis revealed uniform surfaces and abrasive marks. Differences in morphology between treatment conditions, grinding, tumble finished, chemically polished, and laser polished samples, were evaluated.

2.2.3 Nano indentation

To investigate the local (sub-surface) mechanical response of specimens to surface treatments, nanoindentation tests were carried out using a Hysitron TI 950 TriboIndenter® (Bruker Nano Surfaces, USA), as shown in Figure 23. This advanced instrument utilizes capacitive transducer technology and a Performech® Advanced Control Module, offering ultra-high sensitivity and low-noise performance, with force and displacement resolution down to <2 nN and <0.02 nm, respectively. These capabilities enable precise characterization of both hard and soft materials, including metallic systems such as titanium alloys[187].

Figure 23 Hysitron TI 950 TriboIndenter® (Bruker Nano Surfaces, USA)

Samples already were sectioned and embedded in cold-mount epoxy to ensure rigid support. The surfaces were progressively polished using SiC abrasive papers and diamond suspensions down to 0.03 μm. Final polishing was followed by cleaning in an ultrasonic ethanol bath for 10 minutes.

A Berkovich diamond indenter (three-sided pyramidal geometry) was employed for all tests (Figure 24). The loading and unloading curve is depicted in Figure 25. Indentations were performed in a grid pattern with at least 20 repetitions per condition. Spacing between indents was kept at least 10 μm to avoid overlapping of plastic deformation zones.

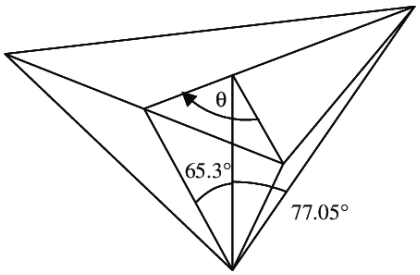

Figure 24 Schematic of a Berkovich indenter tip

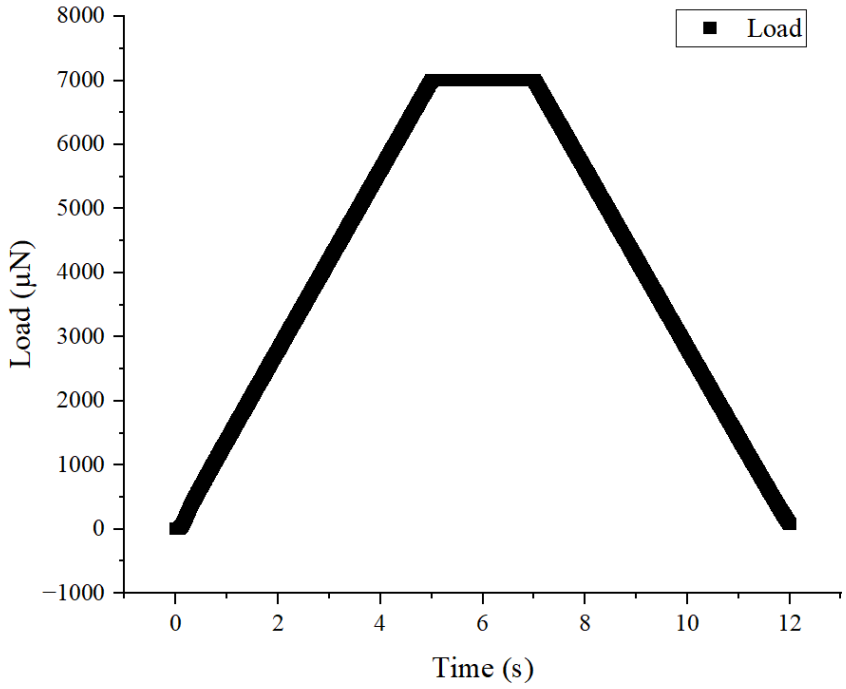

Figure 25 Load–displacement curve illustrating the conditions of the nanoindentation tests

The hardness (*H*) and reduced elastic modulus (*Er*) were derived from the load-displacement curves using the Oliver-Pharr method [188]:

$$H = P_{max} / Ac$$

$$E_r = \left(\frac{\sqrt{\pi}}{2\beta}\right).\left(\frac{S}{\sqrt{A_c}}\right)$$

where:

- P_{max} = Maximum applied load (mN),
- A_c = Projected contact area (nm²), calculated via the tip area function,
- S = Contact stiffness (mN/nm), extracted from the unloading curve slope,
- β = Geometric correction factor (*~1.034 for Berkovich tip*).

The elastic modulus of the sample (E_s) was calculated from E_r by accounting for the indenter's modulus (E_i = 1141 GPa for diamond) and Poisson's ratio (ν_i = 0.07), assuming a sample Poisson's ratio (ν_s) of [0.3 for metals]:

$$1/E_r = (1 - \nu_s^2)/E_s + (1 - \nu_i^2)/E_i$$

Nanoindentation-derived hardness and modulus values were used to estimate wear resistance through the H/E_r ratio (elastic strain to failure) and H^3/E_r^2 (resistance to plastic deformation) [189]:

Wear resistance indicators:

$$\frac{H}{E_r} \text{ and } \frac{H^3}{{E_r}^2}$$

Higher H/E_r ratios (>0.1) suggest improved elasticity and crack resistance, while elevated H^3/E_r^2 values correlate with enhanced resistance to abrasive wear.

3 Results and Discussion

3.1 Overview

This section presents a comprehensive analysis of the effects of L-PBF process parameters and various surface post-treatment methods on the surface quality, morphology, and near-surface mechanical properties of Ti-6242 alloy components. First, the results from the process optimization stage are discussed, including relative density measurements obtained via tomography and Archimedes' methods, as well as initial surface roughness quantification. The influence of process settings, density, and roughness value is examined to identify optimal fabrication parameters. Following this, the effectiveness of four distinct post-processing techniques—grinding, tumble finishing, laser polishing, and chemical polishing—is evaluated based on surface roughness (Ra), SEM micrographs, and surface profilometry. The roughness profiles provide insight into the underlying mechanisms of each treatment, including plastic deformation, material removal, and thermal smoothing. Additionally, nanoindentation results are explored to assess subsurface mechanical behavior, including hardness, elastic modulus, and derived wear resistance indicators (H/Er and H^3/Er^2). Together, these findings provide a holistic understanding of how both process design and surface finishing influence the final performance characteristics of additively manufactured Ti-6242 components.

3.2 Parameter optimization for L-PBF

Material density is generally influenced by the applied volumetric energy density, which in turn is controlled by laser power, laser scanning speed, and the hatch distance. The parameters selected for this study are shown in Figure 26 with the constant of hatch distance equal to 80 µm. The average measured material density, by Archimedes' method, values, presented in Figure 27, varied between 4.49 g/cm³ and 4.51 g/cm³, translating to relative densities ranging from approximately 99.1% to 99.4% of the theoretical Ti-6242 density (4.54 g/cm³). The sample 1 [P=180W; V=1000 (mm/s); VED=75 [J/mm^3]], sample 3 [P=180W; V=1400 (mm/s); VED=53,6 [J/mm^3]]and sample 4 [P=200W; V=1000 (mm/s); VED=83.3 [J/mm^3]] shows the highest Archimedes density among the other samples.

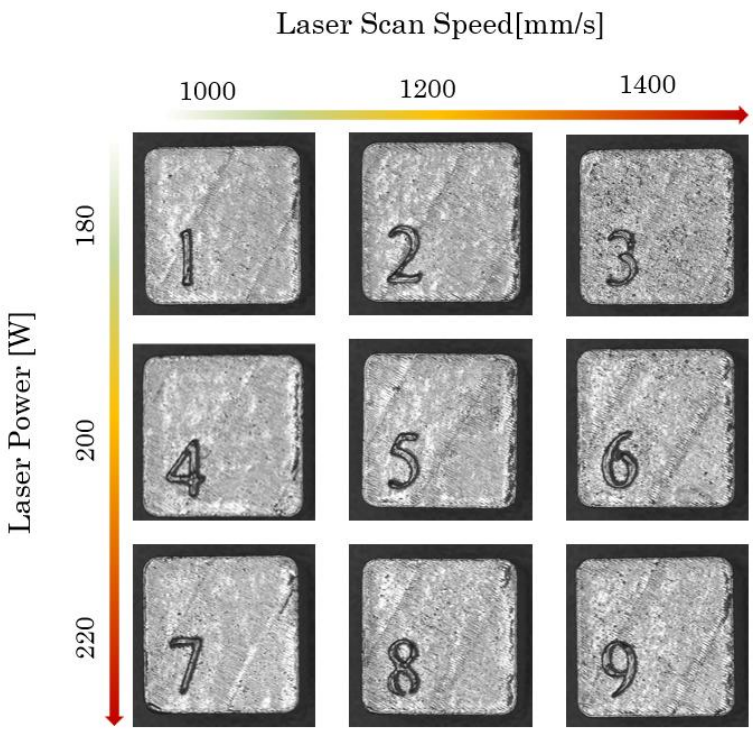

Figure 26 L-PBF samples of Ti-6242 under the DOE parameters

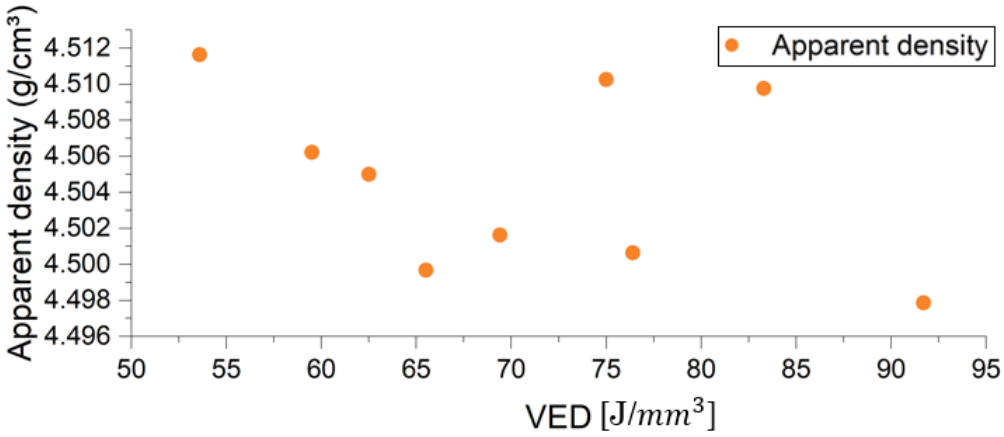

Figure 27 Apparent density of the DOE samples versus VED

X-ray computed tomography was used to quantify internal porosity morphology and distribution in samples. Figure 28 is demonstrating samples processed at lower energy densities revealed irregular; elongated pores typically associated with incomplete fusion between layers. In contrast, samples fabricated with higher energy densities exhibited smaller, spherical pores, characteristic of keyholing or trapped gas phenomena. The total porosity fraction varied from 0.2% to 0.5%, with the lowest porosity observed in samples 1, 3 and 4, corresponding to the densest samples.

Notably, no significant pore clustering was observed, indicating consistent powder spreading and energy delivery during fabrication.

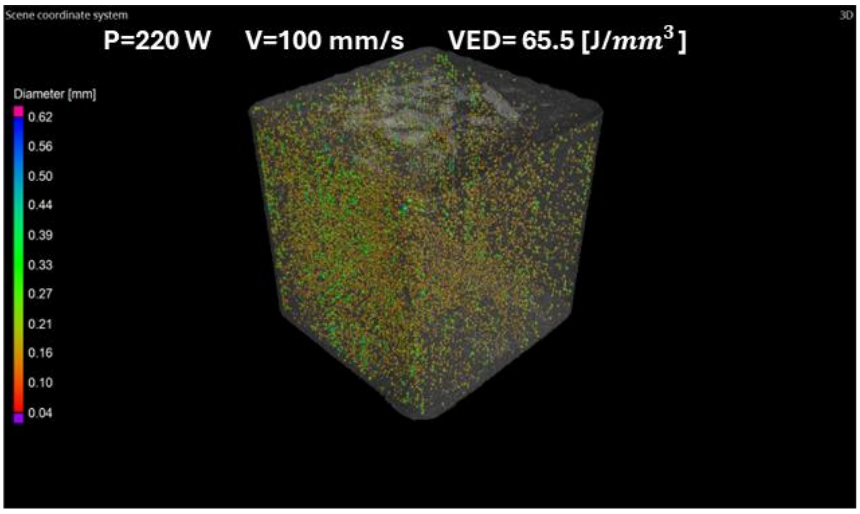

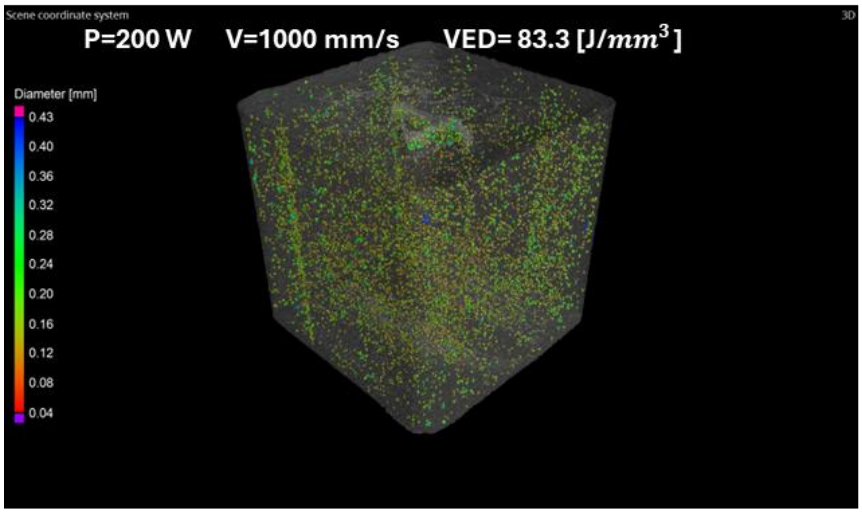

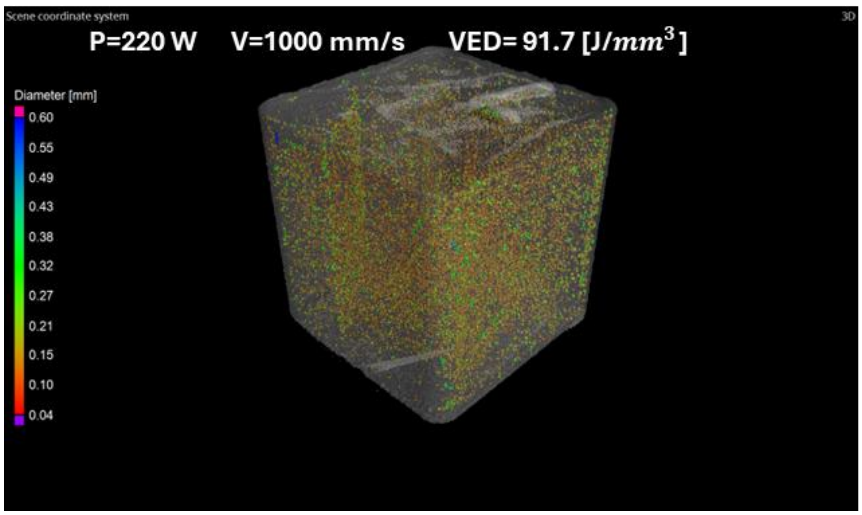

Figure 28 X-ray tomography of DOE samples with different parameters

Figure 29 compares the relative density results obtained from both tomography analysis and the Archimedes method. A consistent trend is observed in the variation of relative density across the different samples using both techniques. However, it is evident that the density values measured by tomography are consistently higher than those obtained via the Archimedes method. This discrepancy can be attributed to the inherent surface roughness of L-PBF-fabricated parts. In the Archimedes method, surface irregularities hinder complete wetting by the liquid medium, leading to measurement inaccuracies and potentially underestimating the actual density. In contrast, X-ray computed tomography enables high-resolution, three-dimensional analysis, allowing for more precise identification of the part boundaries and exclusion of surface artifacts, thereby providing a more accurate estimation of the true material density.

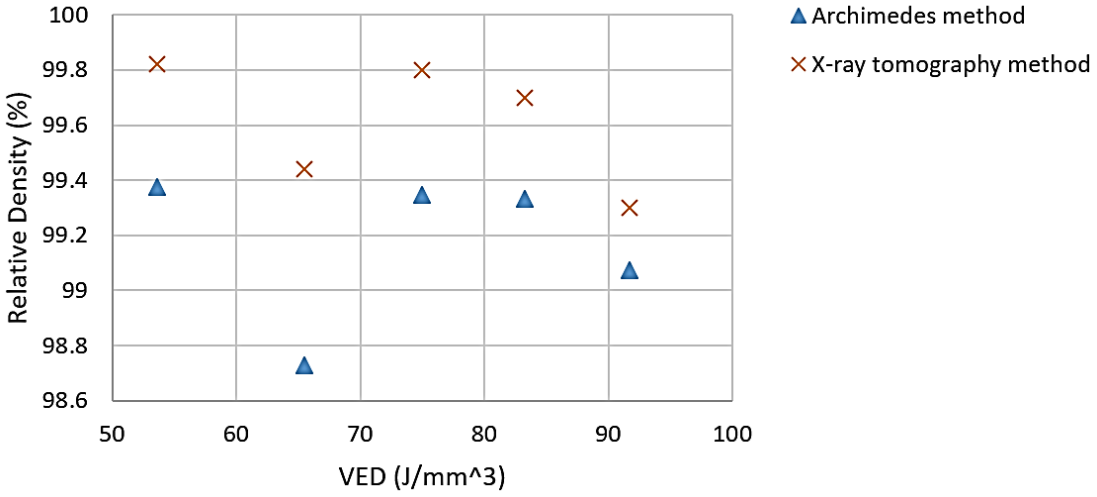

Figure 29 The relative density results obtained from tomography analysis and the Archimedes method

Surface roughness was quantified using contact profilometry, with measured arithmetic average roughness (Ra) values ranging from 3.1 µm to 7.6 µm, as shown in Figure 30. In general, higher scan speeds and lower energy densities are known to increase surface roughness due to the presence of partially melted particles and balling phenomena along the scan tracks. However, in this study, the selected process window was relatively narrow, limiting the ability to observe clear correlations between processing parameters and surface finish. Despite achieving Ra values below 10 µm, which are considered acceptable for minimizing extensive post-processing, surface post-treatments remain essential to meet the stringent quality and performance requirements of high-

performance Ti-6242 components. Surface finishing techniques can further reduce roughness, remove loosely bound particles, and improve fatigue resistance, especially in critical applications.

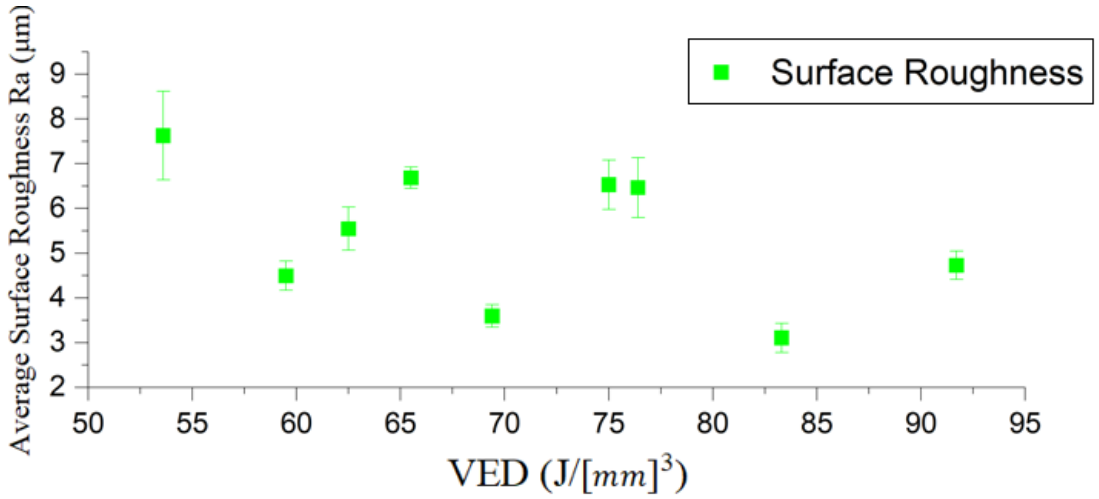

Figure 30 Average Surface Roughness (Ra) vs. VED (J/mm^3) in DoE Process Optimization

The surface roughness profile provides valuable insight into the topographical features resulting from the layer-wise melting and solidification characteristic of the L-PBF process. The measured roughness profiles for the samples with the highest relative densities are presented in Figure 31. These profiles exhibit the presence of irregular peaks and valleys, commonly associated with partially fused powder particles, balling effects, and scan track overlaps. Such surface features contribute to elevated Ra values and reflect the inherent non-uniformity in surface finish under different process conditions. In samples 1 and 3 (Figure 31-A and 31-B), sharp lumps were evident. These are likely to be due to incomplete melt pool fusion or spatter redeposition, which disrupt the smoothness of the top surface. In contrast, Sample 4 (Figure 31-C), produced under a slightly higher energy input, a narrower range of roughness variation, indicative of more complete melting and better material flow during solidification. However, it is important to note that due to the limited range of process parameters explored in this study, no clear or definitive correlation could be established between the specific parameter sets and the resulting surface roughness morphology. Nevertheless, comparative analysis suggests that even moderate increases in energy input can lead to noticeable improvements in surface topography.

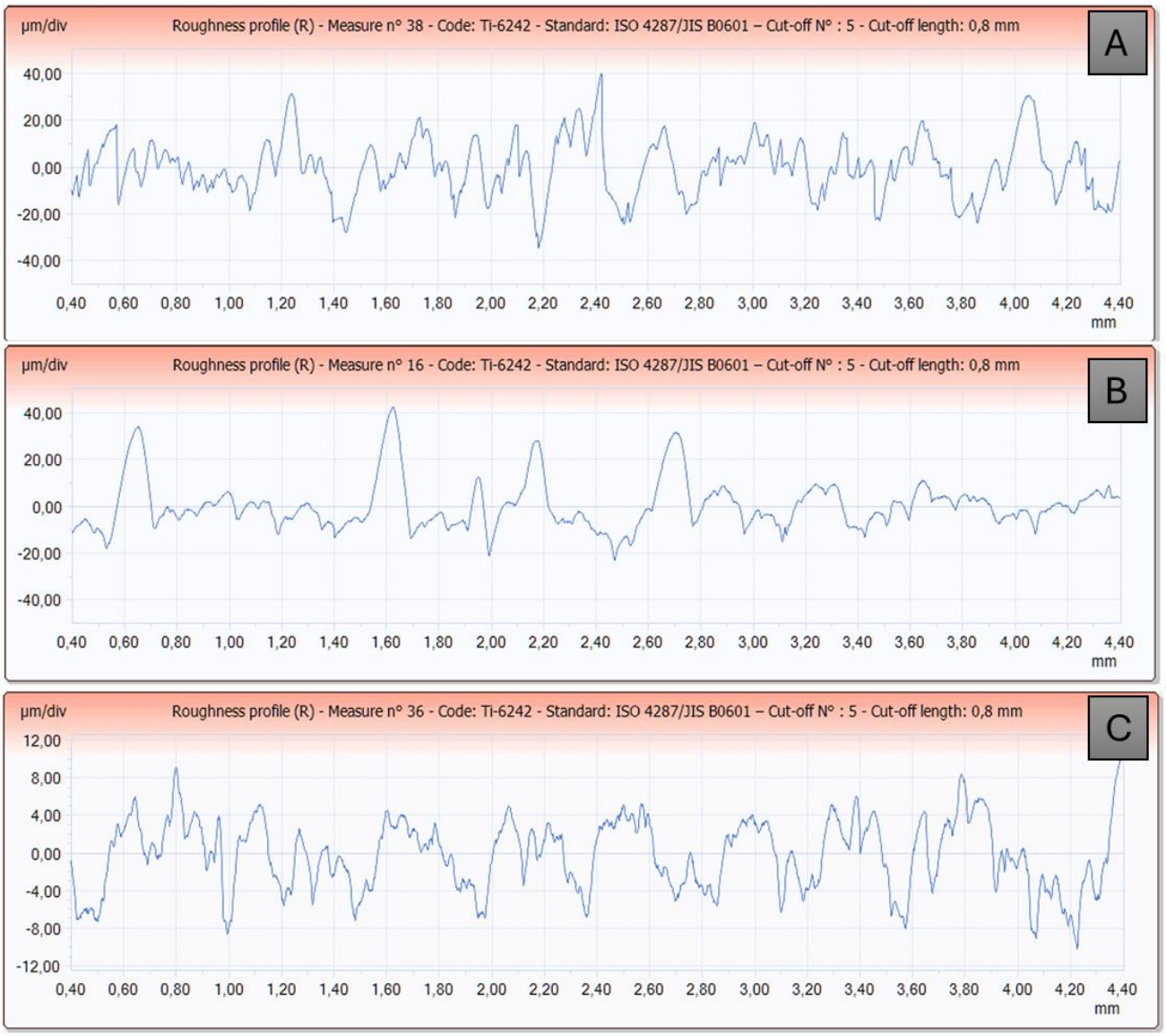

Figure 31Roughness profile of the A) sample 1 [P=180W; V=1000 (mm/s); VED=75 [J/〖mm〗^3]], B) sample 3 [P=180W; V=1400 (mm/s); VED=53,6 [J/〖mm〗^3]], A) sample 4 [P=200W; V=1000 (mm/s); VED=83.3 [J/〖mm〗^3]

Based on the experimental results, sample 4 with VED equal to 83.3 [J/mm^3] exhibited the lowest surface roughness combined with a relatively high material density, these indicated in Figure 32, making it the most favorable among the tested parameter sets. These characteristics indicate a lower defect density in bulk and an improved surface, which are critical for achieving high surface quality, can be achieved in the as-built state. Therefore, the processing parameters used for sample

4 were selected as the optimum condition for manufacturing specimens intended for subsequent surface post-treatment studies.

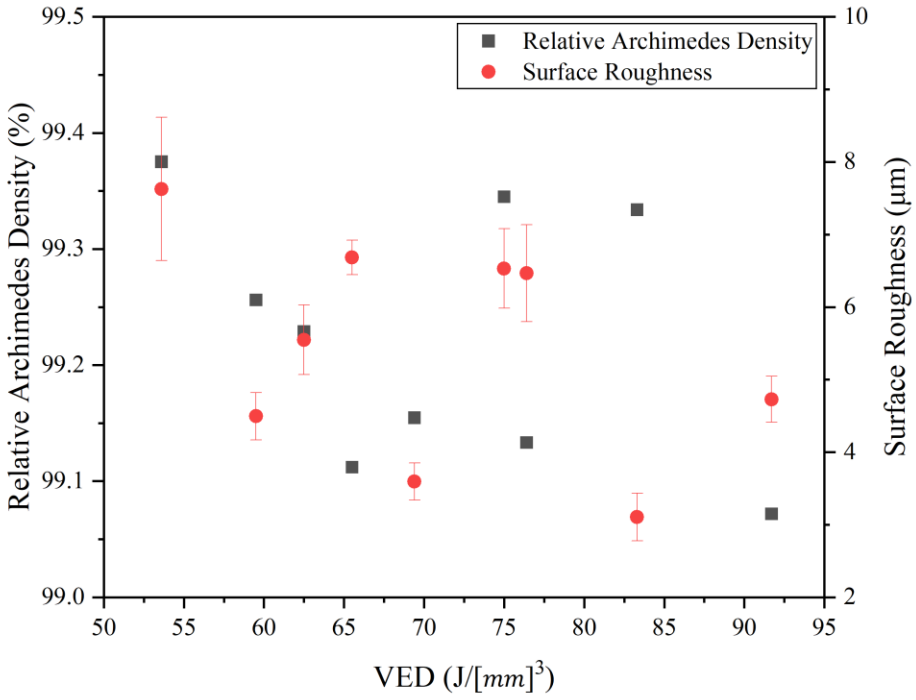

Figure 32 Relative density and Surface roughness of DoE samples based on VED

3.3 Impact of Surface Post-Treatments on Roughness and Morphology

The surface morphology of the as-built metallic AM components showed a high initial surface roughness, which can directly be seen and evaluated after the manufacturing process. Figure 33 displays SEM micrographs of the surface of an as-built plate at two different magnifications. The micrograph reveals partially molten powder particles that remain attached to the surface, and signs of spattering and laser tracks can obviously be observed. Preliminary tests indicated that these particles could not be removed by using an ultrasonic bath. As a result of these particles, the surface exhibits an irregular, rough, and inconsistent morphology.

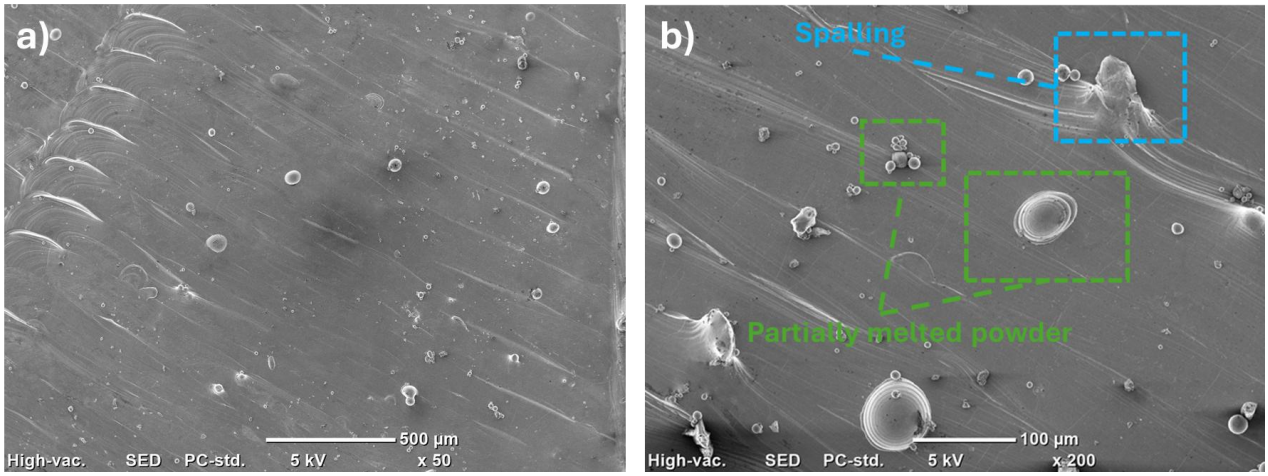

Figure 33 SEM micrographs of as-built top surface showing surface features, a) with x50 magnification b) x200 magnification

Figure 34 demonstrates high roughness values for the as-built top surface and side surface with respect to build direction of material. The standard guidelines for the surface qualities for aerospace applications typically call for a roughness of lower than Ra = 3.2 µm. Notably, the side surfaces which are more prone to stair-step effects and overhanging geometries, tended to show higher Ra values compared to the horizontal top surfaces.

After the surface post-treatment, all methods led to a reduction in surface roughness (Ra), though the degree of improvement varied depending on the mechanism of each process. Figure 35 presents the Ra values before and after treatment. Grinding achieved the most substantial roughness reduction, followed by tumble finishing, laser polishing, and chemical polishing. Mechanically driven treatments were more aggressive in removing surface irregularities, while non-mechanical methods led to slighter changes.

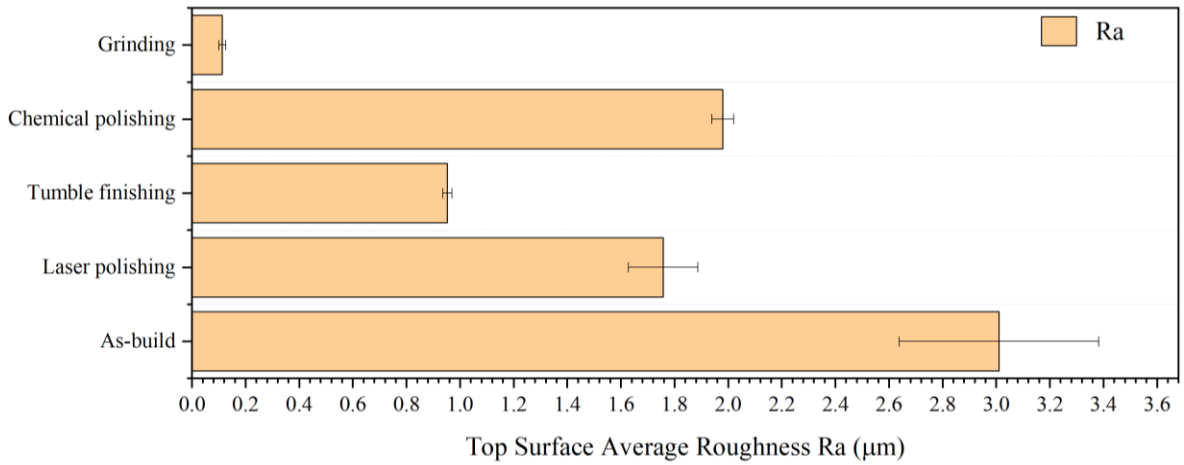

Figure 34 Average surface roughness of as-built and surface post-treated parts on the top surface

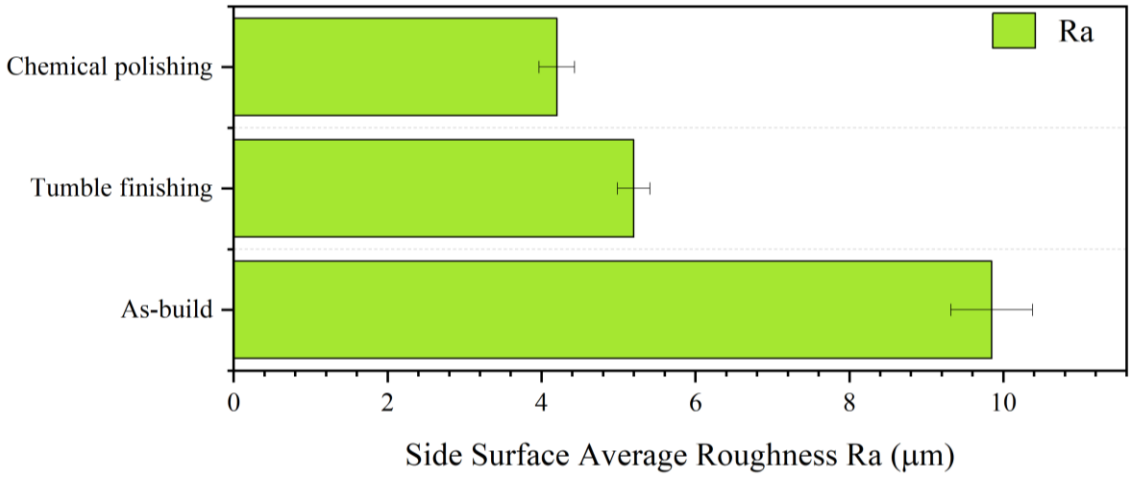

Figure 35 Average surface roughness of as-built and surface post-treated parts on the side surface

SEM images (Figure 36) and corresponding roughness profiles (Figure 37) reveal the distinct effects of each post-treatment method on the surface morphology of L-PBF Ti-6242 components. Grinding produced the smoothest and most uniform surface, characterized by consistent, shallow peaks and valleys. The repeatable pattern observed in the roughness profile reflects the controlled mechanical abrasion typical of this method. Tumble finishing, while slightly less aggressive than grinding, was effective in removing sharp asperities and detaching loosely bound powder particles by locally intense plastic deformation and rubbing of the unfused powder particles. The resulting surfaces exhibited broader valleys and a more randomized topography, which can be attributed to the stochastic nature of media-surface interactions inherent to this method. This random smoothing contributes to an overall reduction in roughness, though with more variability in the surface profile. Laser polishing generated a periodic, wave-like surface texture aligned with the laser scan tracks. Localized remelting and re-solidification led to a significant reduction in surface roughness while eliminating partially fused particles. However, the resulting morphology was influenced by the laser's path, producing a directional surface finish. This controlled reflow of material not only smooths the surface but also creates a more continuous surface layer, potentially enhancing corrosion resistance and surface strength. Chemical polishing, in contrast, resulted in the least reduction in Ra among the treatments. Despite its lower efficacy in smoothing, it preserved the original topographical pattern of the as-built surface, albeit at reduced amplitude. The surface morphology appeared similar in shape to the untreated sample, indicating uniform and isotropic material removal without mechanically altering the surface geometry. This mild etching behavior allows for selective material dissolution while minimizing distortion or surface damage.

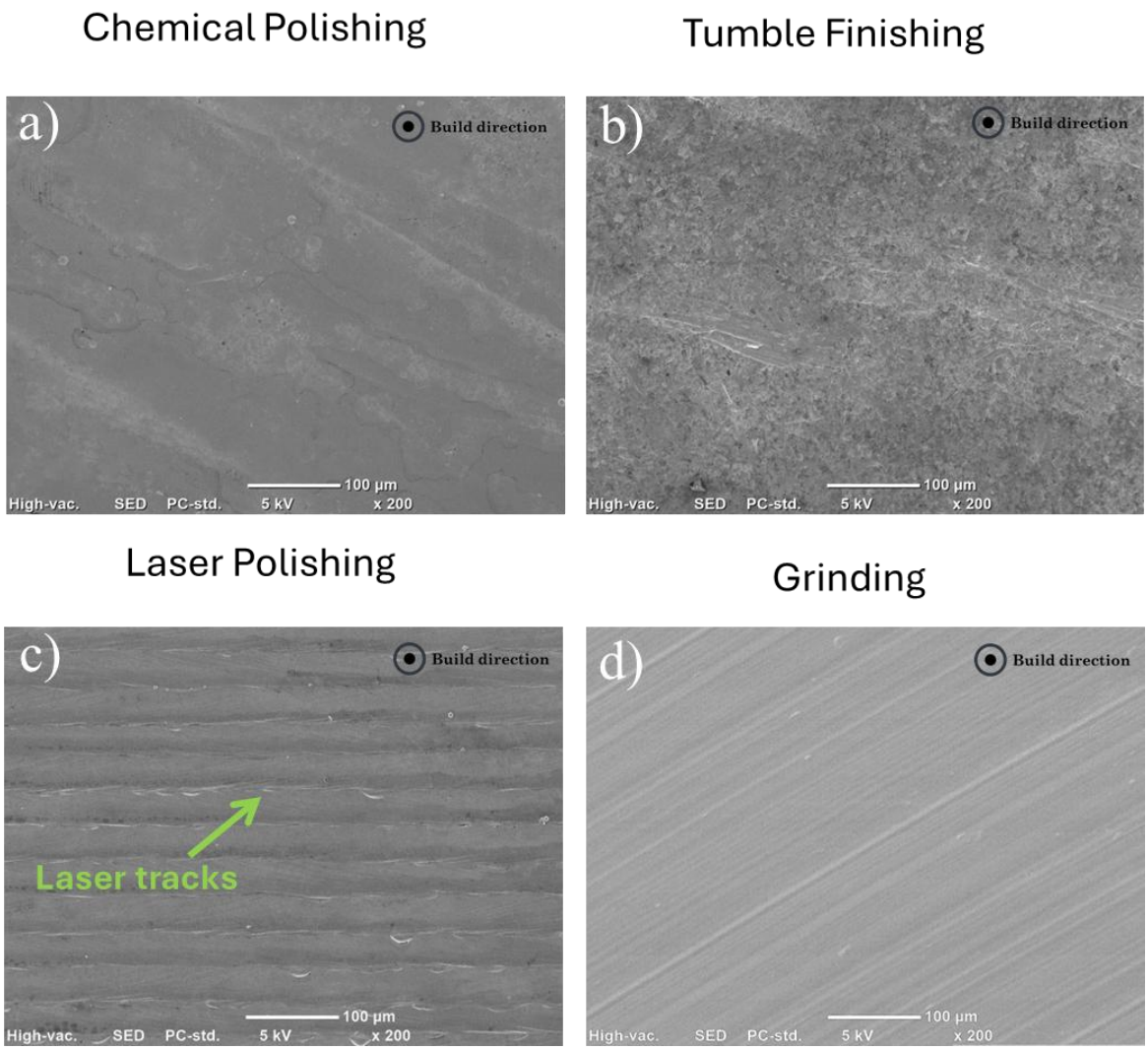

Figure 36 SEM micrograph of top surface of the L-PBF Ti-6242 parts after post treatments

The roughness profiles in Figure 37 provide further insight into these differences. Grinding and laser polishing yielded regular, consistent profiles, indicating uniform material removal across the surface. In contrast, tumble finishing showed less predictable profiles with wider valleys and smoother peaks, characteristic of its more random mechanical action. Chemical polishing maintained the underlying form of the as-built surface but with significantly reduced peak heights and valley depths, confirming its non-deforming, chemically driven mechanism.

Across all treatments, one consistent outcome was the complete removal of partially fused powder particles features that are known to act as critical sites for fatigue crack initiation and corrosion attack. Their elimination enhances not only the aesthetic and dimensional qualities of the part but also its mechanical and environmental performance.

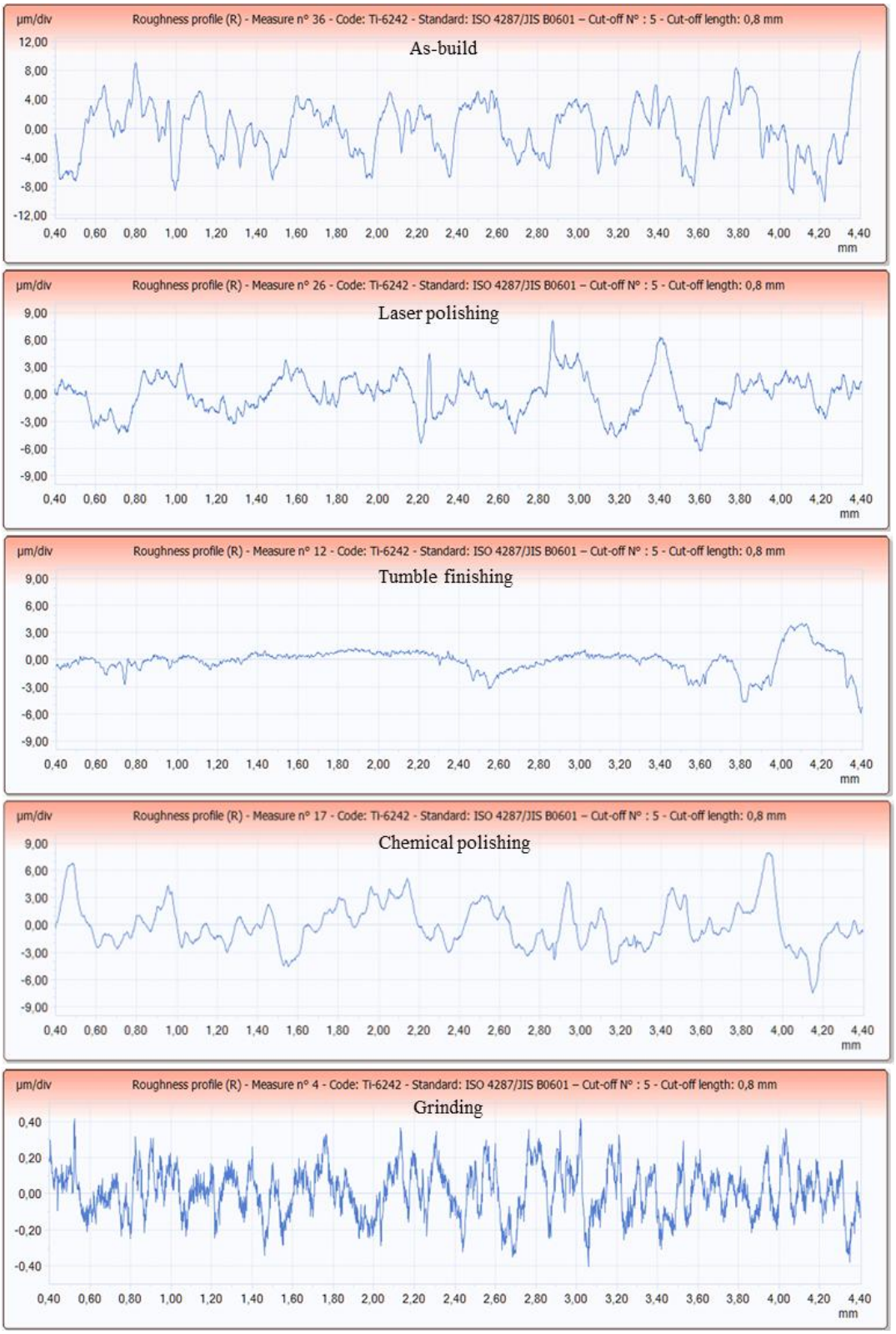

Figure 37 The roughness profile of the parts top surface in as-built state and after surface post-treating of L-PBF samples of Ti-6242 alloy

In addition to their effects on the top surface, tumble finishing and chemical polishing significantly impacted the sidewalls of the L-PBF Ti-6242 parts. Unlike grinding and laser polishing, which are inherently localized treatments applied selectively to accessible or flat regions, tumble and chemical polishing act globally on the entire surface. The abrasive media in tumble finishing interacts with all exposed surfaces during the vibratory cycle, smoothing both horizontal and vertical regions. This led to a noticeable reduction in roughness and partial rounding of sharp edges on the sidewalls, Figure 38-b. Similarly, chemical polishing, being a diffusion- and reaction-based process, uniformly etched all surfaces in contact with the chemical solution. The sidewalls exhibited a reduction in peak height and surface texture amplitude while retaining the as-built morphological signature at a lower scale. These global effects are particularly advantageous for complex geometries or internal channels where direct mechanical, or laser access is limited.

Remarkably, chemical polishing resulted in a slightly lower surface roughness on the sidewalls compared to tumble finishing, shown in Figure 35. This can be attributed to the enhanced reactivity of the exposed, high-surface-area sidewall due to more rough surface with the etchant solution. The morphology likely promotes localized dissolution, leading to more effective smoothing through material removal rather than deformation. In contrast, the sidewalls appear more resistant to mechanical modification via tumble finishing, possibly due to limited abrasive contact and lower pressure exerted on vertical features, resulting in comparatively higher residual roughness.

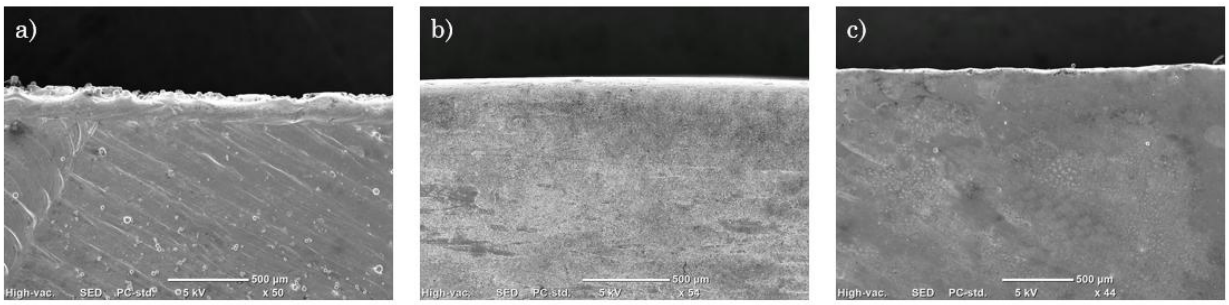

Figure 38 The SEM micrograph of the edge of top surface of TI-6242, L-PBF parts, showing morphology of the side walls in a) as-build state b)tumble finished, c) chemical polished

The roughness profiles of the sidewalls before and after post-processing are presented in Figure 39. Similar to the top surface, tumble finishing results in a significant reduction of surface peaks and the formation of broader valleys. This is primarily due to localized plastic deformation and abrasive contact, which effectively removes loosely bonded or unfused powder particles. In contrast, chemical polishing produces a profile that closely resembles the as-built surface in overall shape but with markedly reduced peak and valley amplitudes. The chemical etching action not only lowers the roughness of the surface but also smooths the contours of the surface features, leading to more rounded peak geometries. These observations underscore the differing

mechanisms of the two treatments, mechanical abrasion versus uniform material dissolution, and their distinct impacts on surface topography.

Figure 39 The roughness profile of the side walls of the parts in as-built state, tumble finished, and chemical polished

3.4 Impact of Surface Post-Treatments on Nano-indentation Hardness

The nanoindentation load–depth curves for the as-built and post-treated Ti-6242 samples, Figure 40, reveal the surface and near-surface mechanical response under localized compressive loading. The curves for the as-built, ground, and chemically polished surfaces showed similar maximum indentation depths and unloading slopes, suggesting minimal or no alteration in subsurface mechanical properties. This indicates that these treatments primarily affected surface topography without significantly modifying microstructural hardness. In contrast, the laser-polished sample exhibited a noticeably deeper indentation depth and a broader curve, indicative of localized softening due to surface remelting and structural relaxation. Meanwhile, the tumble-finished sample displayed a slightly shallower depth, consistent with increased hardness due to strain hardening from mechanical impact during processing.

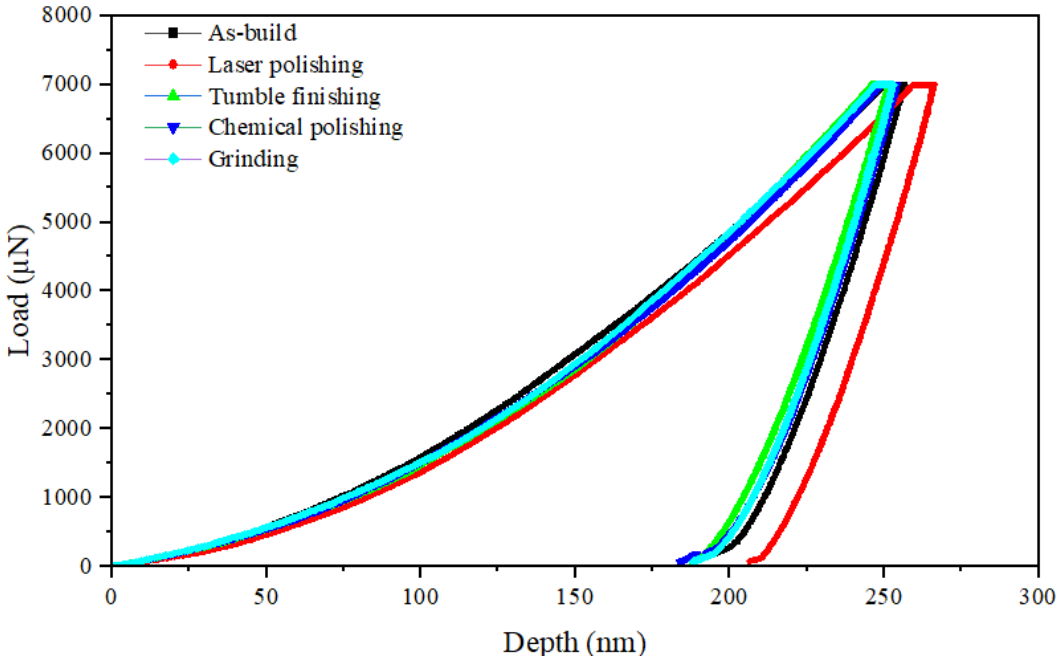

Figure 40 Loading and unloading curves of nanoindentation for as-built and post-treated samples

The depth-profiled nanoindentation hardness in Figure 41 measurements revealed how different post-treatments influenced the near-surface mechanical properties of Ti-6242. The as-built, ground, and chemically polished samples exhibited nearly identical hardness trends as a function of depth, indicating that these treatments had a negligible effect on subsurface strengthening or softening. In contrast, the tumble-finished surface showed a distinct hardness increase between ~30 μm and 20 μm beneath the surface up to surface, suggesting the presence of a strain-hardened layer induced by mechanical impacts during processing. On the other hand, the laser-polished

sample exhibited a gradual reduction in hardness extending to a depth of approximately 130 µm below the surface.

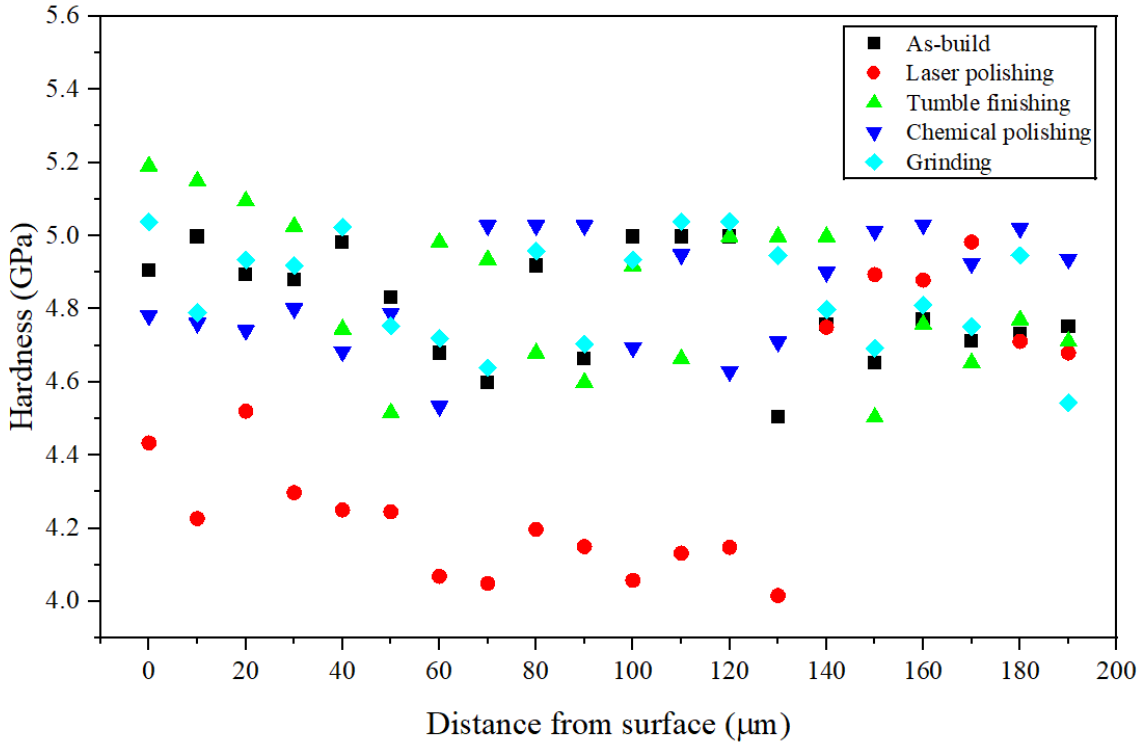

Figure 41 The depth-profiled nanoindentation hardness of as-built and surface post-treated samples

Nanoindentation measurements of hardness (H) and reduced modulus (Er) confirmed the trends observed in the load–displacement curves, demonstrate in Figure 42. The as-built, grinding, and chemically polished samples showed comparable hardness and modulus values, suggesting that grinding and chemical polishing, while effective in altering surface roughness, did not significantly influence the subsurface mechanical response. Tumble finishing resulted in a slight increase in hardness, likely due to plastic deformation and strain hardening at the surface caused by repeated mechanical abrasion. In contrast, the laser-polished surface showed a reduction in both hardness and Er, which can be attributed to localized melting and re-solidification during the process. This thermal effect may lead to microstructural relaxation or grain growth, reducing resistance to plastic deformation beneath the polished surface.

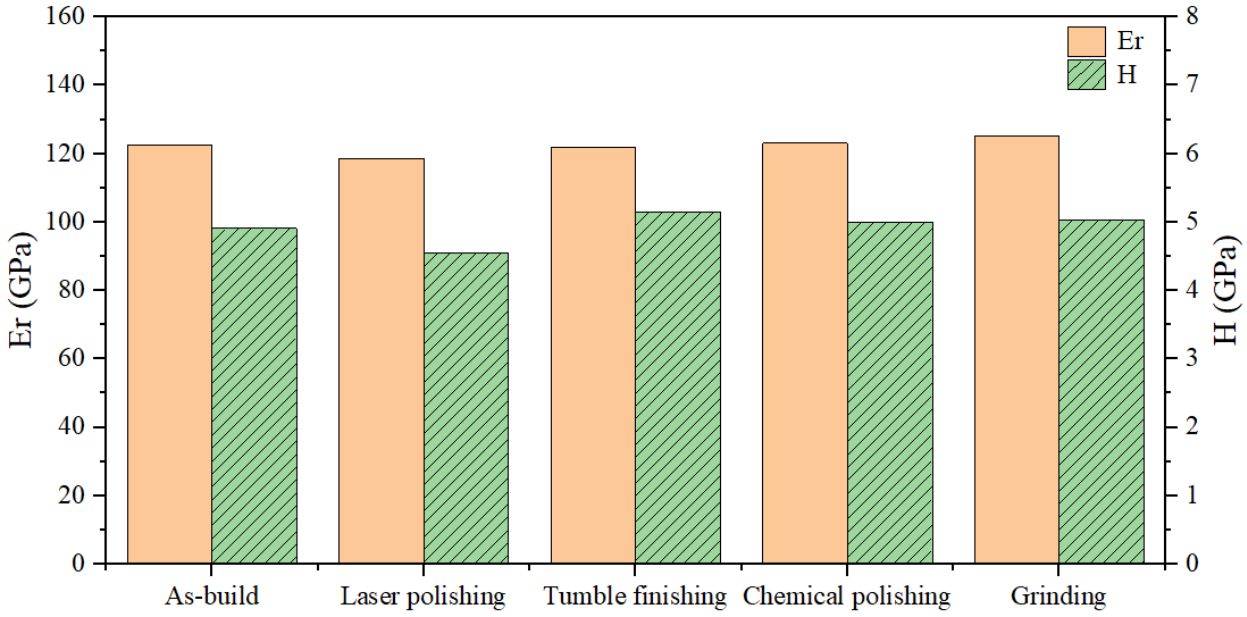

Figure 42) The hardness (H) and reduced elastic modulus (Er) of as-built and surface post-treated samples

To assess wear resistance, the hardness-to-modulus ratio (H/Er) and plasticity index (H^3/Er^2) were calculated from the nanoindentation data, presented in Figure 43. These indicators reflect a material's ability to resist plastic deformation and accommodate elastic strain. Tumble-finished samples exhibited the highest values for both H/Er and H^3/Er^2, indicating improved wear resistance due to surface hardening. The as-built, ground, and chemically polished surfaces demonstrated similar wear resistance metrics, reflecting their shared mechanical behavior beneath the surface. Laser-polished samples, despite improved surface smoothness, exhibited the lowest values of H/Er and H^3/Er^2. This reduction aligns with the observed decrease in hardness and modulus and suggests that surface melting may compromise the wear performance. Overall, these results highlight the

trade-off between surface quality and mechanical integrity introduced by different post-processing strategies.

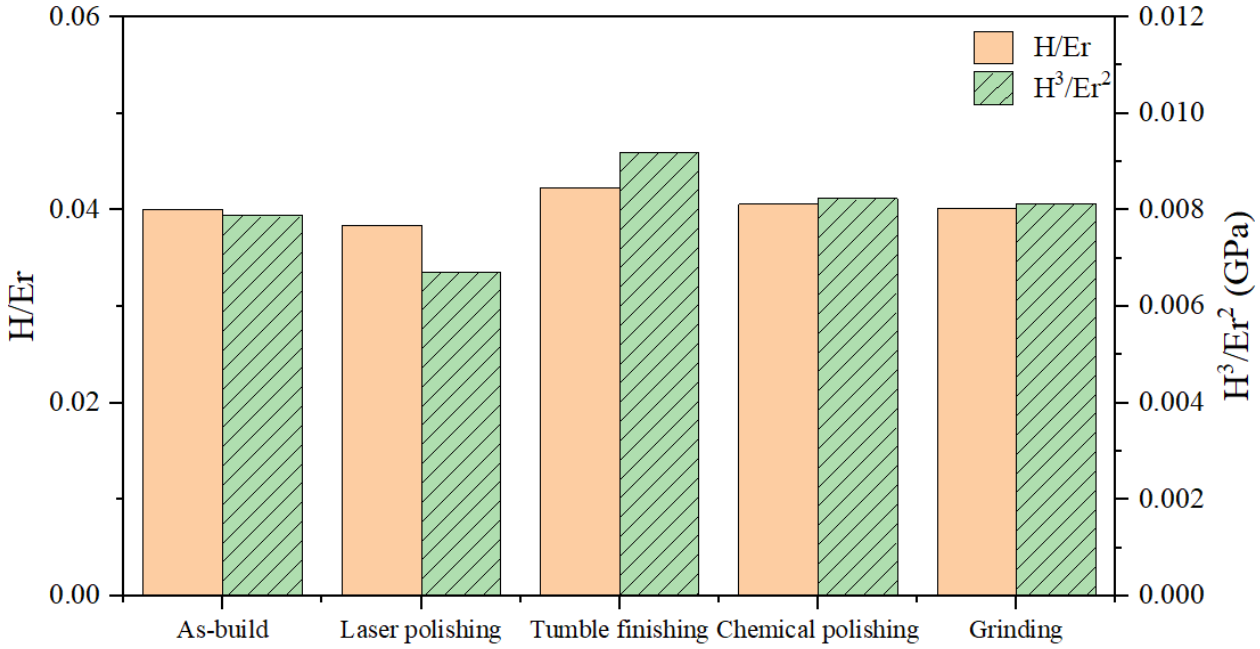

Figure 43 The H/Er and H³/Er² ratio for as-built and surface post-treated samples

4 Conclusion and Future Perspectives

This study comprehensively investigated both the process parameter optimization and the effect of surface post-treatment techniques on the surface quality and near-surface mechanical properties of Ti-6242 alloy components fabricated via L-PBF.

Through a DOE approach, key process parameters, laser power and laser scanning speed, were systematically varied to identify optimal combinations that maximize material density and minimize surface roughness. Among the nine parameter sets evaluated, sample 4 [P=200W; V=1000 (mm/s); VED=83.3 [J/mm^3], processed at moderate energy input conditions, achieved the highest relative density and the lowest initial surface roughness. This parameter set was thus selected as the optimal condition for subsequent surface post-treatment investigations. The observed improvements are attributed to a balanced energy density that enabled sufficient powder consolidation without inducing excessive spatter or surface irregularities.

Following optimization, four post-processing methods—grinding, tumble finishing, laser polishing, and chemical polishing—were applied to the as-built Ti-6242 specimens. All techniques

led to a notable decrease in surface roughness (Ra), albeit with different surface morphologies and material responses. Grinding provided the most significant roughness reduction, producing a uniform surface with shallow, repeatable features ideal for fatigue-critical applications. Tumble finishing effectively removed loose particles and smoothed asperities while introducing plastic deformation, which slightly increased subsurface hardness. Laser polishing, while successful in eliminating partially fused particles, led to reduced hardness and elastic modulus beneath the surface due to thermal relaxation and remelting effects. Chemical polishing preserved the surface geometry of the as-built material while achieving modest roughness reduction through isotropic, non-deforming material removal.

Surface roughness profile analysis revealed distinct textural signatures associated with each treatment. Grinding and laser polishing generated periodic profiles with consistent topography, while tumble finishing resulted in broader valleys and smoothed peaks due to media-surface interactions. Chemical polishing maintained the overall profile shape but reduced its amplitude, reflecting uniform etching action. Notably, sidewalls, which are inherently rougher due to powder adhesion and build orientation, responded effectively to chemical and tumble polishing despite the localized treatments like grinding and laser polishing.

Nanoindentation testing provided insight into the mechanical response just beneath the surface. Grinding and chemical polishing treatments preserved the hardness and reduced modulus of the as-built material, except for laser polishing, which caused a decline in both properties up to ~130 μm from the surface. Conversely, tumble finishing induced localized strain hardening, increasing hardness between 20–30 μm below the surface. Wear resistance indicators, including H/Er and H^3/Er^2, supported these findings, with tumble-finished surfaces showing enhanced resistance due to work-hardening, and laser-polished ones reflecting lower resistance due to microstructural relaxation.

This work highlights the importance of coupling process parameter optimization with tailored surface finishing in achieving high-performance Ti-6242 components for demanding applications, particularly in aerospace. Future research should focus on the following:

Microstructural characterization (e.g., EBSD, TEM) to link subsurface modifications to phase transformation and grain structure.

Fatigue and corrosion testing to assess long-term reliability of post-treated surfaces.

Hybrid surface treatment strategies, combining mechanical and chemical or thermal methods for synergistic effects.

Process scalability and industrial integration, to evaluate the economic and practical viability of optimized L-PBF and post-treatment routes for critical components.

In conclusion, the combined optimization of L-PBF parameters and surface treatment strategies demonstrates a promising path toward producing Ti-6242 parts with both high densification and tailored surface integrity, ready for qualification in structural and aerospace-grade applications.

5 References

[1] T. Barbin *et al.*, "3D metal printing in dentistry: An in vitro biomechanical comparative study of two additive manufacturing technologies for full-arch implant-supported prostheses," *J Mech Behav Biomed Mater*, vol. 108, p. 103821, Aug. 2020, doi: 10.1016/J.JMBBM.2020.103821.

[2] M. R. Bandekhoda, M. H. Mosallanejad, M. Atapour, L. Iuliano, and A. Saboori, "Investigation on the Potential of Laser and Electron Beam Additively Manufactured Ti–6Al–4V Components for Orthopedic Applications," *Metals and Materials International*, vol. 30, no. 1, pp. 114–126, Jan. 2024, doi: 10.1007/S12540-023-01496-6/FIGURES/11.

[3] J. C. Williams and R. R. Boyer, "Opportunities and Issues in the Application of Titanium Alloys for Aerospace Components," *Metals 2020, Vol. 10, Page 705*, vol. 10, no. 6, p. 705, May 2020, doi: 10.3390/MET10060705.

[4] V. Juechter, M. M. Franke, T. Merenda, A. Stich, C. Körner, and R. F. Singer, "Additive manufacturing of Ti-45Al-4Nb-C by selective electron beam melting for automotive applications," *Addit Manuf*, vol. 22, pp. 118–126, Aug. 2018, doi: 10.1016/J.ADDMA.2018.05.008.

[5] Z. Liu, S. Xin, and Y. Zhao, "Research Progress on the Creep Resistance of High-Temperature Titanium Alloys: A Review," *Metals 2023, Vol. 13, Page 1975*, vol. 13, no. 12, p. 1975, Dec. 2023, doi: 10.3390/MET13121975.

[6] M. Abdullah, A. Mubashar, E. Uddin, A. Vance, K. Bari, and A. Arjunan, "Investigation of Ti64 sheathed cellular anatomical structure as a tibia implant," *Biomed Phys Eng Express*, vol. 5, no. 3, p. 035008, Mar. 2019, doi: 10.1088/2057-1976/AB0BD7.

[7] F. H. S. Froes, M. N. Gungor, and M. Ashraf Imam, "Cost-affordable titanium: The component fabrication perspective," *JOM*, vol. 59, no. 6, pp. 28–31, 2007, doi: 10.1007/s11837-007-0074-8.

[8] A. Barbas, A. S. Bonnet, P. Lipinski, R. Pesci, and G. Dubois, "Development and mechanical characterization of porous titanium bone substitutes," *J Mech Behav Biomed Mater*, vol. 9, pp. 34–44, May 2012, doi: 10.1016/J.JMBBM.2012.01.008.

[9] D. Eylon, F. H. Froes, and R. W. Gardiner, "Developments in Titanium Alloy Casting Technology," *JOM: Journal of The Minerals, Metals & Materials Society*, vol. 35, no. 2, pp. 35–47, Dec. 1983, doi: 10.1007/BF03338203/METRICS.

[10] A. Arjunan, A. Baroutaji, and A. Latif, "Acoustic behaviour of 3D printed titanium perforated panels," *Results in Engineering*, vol. 11, p. 100252, Sep. 2021, doi: 10.1016/J.RINENG.2021.100252.

[11] F. Bartolomeu, M. Gasik, F. S. Silva, and G. Miranda, "Mechanical Properties of Ti6Al4V Fabricated by Laser Powder Bed Fusion: A Review Focused on the Processing and Microstructural Parameters

Influence on the Final Properties," *Metals 2022, Vol. 12, Page 986*, vol. 12, no. 6, p. 986, Jun. 2022, doi: 10.3390/MET12060986.

[12] J. Gockel, J. Fox, J. Beuth, and R. Hafley, "Integrated melt pool and microstructure control for Ti-6Al-4V thin wall additive manufacturing," *Materials Science and Technology (United Kingdom)*, vol. 31, no. 8, pp. 912–916, Jun. 2015, doi: 10.1179/1743284714Y.0000000704.

[13] A. Carrozza *et al.*, "Effect of Aging and Cooling Path on the Super β-Transus Heat-Treated Ti-6Al-4V Alloy Produced via Electron Beam Melting (EBM)," *Materials 2022, Vol. 15, Page 4067*, vol. 15, no. 12, p. 4067, Jun. 2022, doi: 10.3390/MA15124067.

[14] H. Fan and S. Yang, "Effects of direct aging on near-alpha Ti–6Al–2Sn–4Zr–2Mo (Ti-6242) titanium alloy fabricated by selective laser melting (SLM)," *Materials Science and Engineering: A*, vol. 788, p. 139533, Jun. 2020, doi: 10.1016/j.msea.2020.139533.

[15] S. Sun, M. Brandt, and M. S. Dargusch, "Thermally enhanced machining of hard-to-machine materials—A review," *Int J Mach Tools Manuf*, vol. 50, no. 8, pp. 663–680, Aug. 2010, doi: 10.1016/J.IJMACHTOOLS.2010.04.008.

[16] R. K. Gupta, V. A. Kumar, C. Mathew, and G. S. Rao, "Strain hardening of Titanium alloy Ti6Al4V sheets with prior heat treatment and cold working," *Materials Science and Engineering: A*, vol. 662, pp. 537–550, Apr. 2016, doi: 10.1016/J.MSEA.2016.03.094.

[17] A. V. S. R. Prasad, Koona. Ramji, and G. L. Datta, "An Experimental Study of Wire EDM on Ti-6Al-4V Alloy," *Procedia Materials Science*, vol. 5, pp. 2567–2576, Jan. 2014, doi: 10.1016/J.MSPRO.2014.07.517.

[18] T. S. Jang, D. E. Kim, G. Han, C. B. Yoon, and H. Do Jung, "Powder based additive manufacturing for biomedical application of titanium and its alloys: a review," *SpringerTS Jang, DE Kim, G Han, CB Yoon, HD JungBiomedical engineering letters, 2020•Springer*, vol. 10, no. 4, pp. 505–516, Nov. 2020, doi: 10.1007/S13534-020-00177-2.

[19] "Mehrpouya: Handbooks in Advanced Manufacturing - Google Scholar." Accessed: Jun. 20, 2025. [Online]. Available: https://scholar.google.com/scholar_lookup?hl=en&publication_year=2021&author=M.+Mehrpouya&author=A.+Vosooghnia&author=A.+Dehghanghadikolaei&author=B.+Fotovvati&title=Handbooks+in+Advanced+Manufacturing

[20] P. Moghimian *et al.*, "Metal powders in additive manufacturing: A review on reusability and recyclability of common titanium, nickel and aluminum alloys," *Addit Manuf*, vol. 43, p. 102017, Jul. 2021, doi: 10.1016/J.ADDMA.2021.102017.

[21] G. Del Guercio, M. Galati, A. Saboori, P. Fino, and L. Iuliano, "Microstructure and Mechanical Performance of Ti–6Al–4V Lattice Structures Manufactured via Electron Beam Melting (EBM): A Review," *Acta Metallurgica Sinica (English Letters)*, vol. 33, no. 2, pp. 183–203, Feb. 2020, doi: 10.1007/S40195-020-00998-1/TABLES/6.

[22] B. E. Carroll, T. A. Palmer, and A. M. Beese, "Anisotropic tensile behavior of Ti–6Al–4V components fabricated with directed energy deposition additive manufacturing," *Acta Mater*, vol. 87, pp. 309–320, Apr. 2015, doi: 10.1016/J.ACTAMAT.2014.12.054.

[23] M. J. Bermingham, D. Kent, H. Zhan, D. H. Stjohn, and M. S. Dargusch, “Controlling the microstructure and properties of wire arc additive manufactured Ti–6Al–4V with trace boron additions,” *Acta Mater*, vol. 91, pp. 289–303, Jun. 2015, doi: 10.1016/J.ACTAMAT.2015.03.035.

[24] I. Yadroitsev and I. Smurov, “Surface Morphology in Selective Laser Melting of Metal Powders,” *Phys Procedia*, vol. 12, no. PART 1, pp. 264–270, Jan. 2011, doi: 10.1016/J.PHPRO.2011.03.034.

[25] M. H. Nasab, D. Gastaldi, N. F. Lecis, and M. Vedani, “On morphological surface features of the parts printed by selective laser melting (SLM),” *Addit Manuf*, vol. 24, pp. 373–377, Dec. 2018, doi: 10.1016/J.ADDMA.2018.10.011.

[26] K. W.E. *et al.*, “Laser powder bed fusion additive manufacturing of metals; physics, computational, and materials challenges,” *Volume 2, Issue 4*, Accessed: Jun. 20, 2025. [Online]. Available: https://www.scopus.com/record/display.uri?eid=2-s2.0-84958992852&origin=inward&txGid=5aa9999dadb755ad53e523b299f60378

[27] T. DebRoy *et al.*, “Additive manufacturing of metallic components – Process, structure and properties,” *Prog Mater Sci*, vol. 92, pp. 112–224, 2018, doi: 10.1016/j.pmatsci.2017.10.001.

[28] E. Maleki, O. Unal, and K. Reza Kashyzadeh, “Fatigue behavior prediction and analysis of shot peened mild carbon steels,” *Int J Fatigue*, vol. 116, pp. 48–67, 2018, doi: 10.1016/j.ijfatigue.2018.06.004.

[29] J. W. Pegues *et al.*, “Fatigue of additive manufactured Ti-6Al-4V, Part I: The effects of powder feedstock, manufacturing, and post-process conditions on the resulting microstructure and defects,” *Int J Fatigue*, vol. 132, 2020, doi: 10.1016/j.ijfatigue.2019.105358.

[30] M. H. Mosallanejad, A. Abdi, F. Karpasand, N. Nassiri, L. Iuliano, and A. Saboori, “Additive Manufacturing of Titanium Alloys: Processability, Properties, and Applications,” *Adv Eng Mater*, vol. 25, no. 24, p. 2301122, Dec. 2023, doi: 10.1002/adem.202301122.

[31] M. Vafaei, R. Ghanavati, A. Saboori, and L. Iuliano, “The impact of heat treatment on microstructure, residual stress, and mechanical behavior of laser powder bed fusion additively manufactured Ti–6Al–2Sn–4Zr–2Mo alloy,” *Journal of Materials Research and Technology*, vol. 33, pp. 5731–5743, Nov. 2024, doi: 10.1016/J.JMRT.2024.10.202.

[32] S. E. Haghighi, H. B. Lu, G. Y. Jian, G. H. Cao, D. Habibi, and L. C. Zhang, “Effect of α" martensite on the microstructure and mechanical properties of beta-type Ti–Fe–Ta alloys,” *Mater Des*, vol. 76, pp. 47–54, 2015, doi: https://doi.org/10.1016/j.matdes.2015.03.028.

[33] C. Veiga, J. P. Davim, and A. Loureiro, “Properties and applications of titanium alloys: A brief review,” *Reviews on Advanced Materials Science*, vol. 32, pp. 133–148, Dec. 2012.

[34] W. Abd-Elaziem, M. A. Darwish, A. Hamada, and W. M. Daoush, “Titanium-Based alloys and composites for orthopedic implants Applications: A comprehensive review,” *Mater Des*, vol. 241, p. 112850, May 2024, doi: 10.1016/J.MATDES.2024.112850.

[35] J. Lu and L. Zhuo, “Additive manufacturing of titanium alloys via selective laser melting: Fabrication, microstructure, post-processing, performance and prospect,” *Int J Refract Metals Hard Mater*, vol. 111, p. 106110, 2023, doi: https://doi.org/10.1016/j.ijrmhm.2023.106110.

[36] D. Banerjee and J. C. Williams, “Perspectives on Titanium Science and Technology,” *Acta Mater*, vol. 61, no. 3, pp. 844–879, Feb. 2013, doi: 10.1016/J.ACTAMAT.2012.10.043.

[37] Y. Liu and S. L. Sing, “A review of advances in additive manufacturing and the integration of high-performance polymers, alloys, and their composites,” *Materials Science in Additive Manufacturing 2023, 2(3), 1587*, vol. 2, no. 3, p. 1587, Sep. 2023, doi: 10.36922/MSAM.1587.

[38] L. C. Zhang, L. Y. Chen, S. Zhou, and Z. Luo, “Powder bed fusion manufacturing of beta-type titanium alloys for biomedical implant applications: A review,” *J Alloys Compd*, vol. 936, p. 168099, Mar. 2023, doi: 10.1016/j.jallcom.2022.168099.

[39] A. Sola and A. Trinchi, “Boron-induced microstructural manipulation of titanium and titanium alloys in additive manufacturing,” *Virtual Phys Prototyp*, vol. 18, no. 1, 2023, doi: 10.1080/17452759.2023.2230467.

[40] J. M. Holt, C. Gibson, and C. Y. (Cho Y. Ho 1928-, *Structural alloys handbook*. Indiana, United States: West Lafayette, Ind. : CINDAS/Purdue University, 1999. [Online]. Available: https://searchworks.stanford.edu/view/3303912

[41] F. Hardesty, “Metals handbook, ninth edition. Volume 3, Properties and selection: Stainless steels, tool materials and special-purpose metals,” *Journal of Mechanical Working Technology*, vol. 6, no. 4, pp. 391–393, Jun. 1982, doi: 10.1016/0378-3804(82)90039-0.

[42] A. H. Committee, “Properties and Selection: Nonferrous Alloys and Special-Purpose Materials,” *Properties and Selection: Nonferrous Alloys and Special-Purpose Materials*, Jan. 1990, doi: 10.31399/ASM.HB.V02.9781627081627.

[43] A. Saboori, D. Gallo, S. Biamino, P. Fino, and M. Lombardi, “An Overview of Additive Manufacturing of Titanium Components by Directed Energy Deposition: Microstructure and Mechanical Properties,” *Applied Sciences 2017, Vol. 7, Page 883*, vol. 7, no. 9, p. 883, Aug. 2017, doi: 10.3390/APP7090883.

[44] D. H. Kim and C. M. Lee, “Experimental Investigation on Machinability of Titanium Alloy by Laser-Assisted End Milling,” *Metals 2021, Vol. 11, Page 1552*, vol. 11, no. 10, p. 1552, Sep. 2021, doi: 10.3390/MET11101552.

[45] “ASTM F2792-12a, Standard Terminology for Additive Manufacturing Technologies, ASTM International, 2012.”

[46] B. Dutta and F. H. Froes, “Chapter 1 - The Additive Manufacturing of Titanium Alloys,” in *Additive Manufacturing of Titanium Alloys*, B. Dutta and F. H. Froes, Eds., Butterworth-Heinemann, 2016, pp. 1–10. doi: https://doi.org/10.1016/B978-0-12-804782-8.00001-X.

[47] T. DebRoy *et al.*, “Additive manufacturing of metallic components – Process, structure and properties,” *Prog Mater Sci*, vol. 92, pp. 112–224, Mar. 2018, doi: 10.1016/J.PMATSCI.2017.10.001.

[48] D. Svetlizky *et al.*, “Directed Energy Deposition (DED) Additive Manufacturing: Physical Characteristics, Defects, Challenges and Applications,” *Materials Today*, vol. 49, pp. 271–295, Dec. 2021, doi: 10.1016/j.mattod.2021.03.020.

[49] Z. Liu *et al.*, “Environmental benefits of remanufacturing: A case study of cylinder heads remanufactured through laser cladding,” *J Clean Prod*, vol. 133, pp. 1027–1033, 2016, doi: 10.1016/j.jclepro.2016.06.049.

[50] A. Dass and A. Moridi, “State of the Art in Directed Energy Deposition: From Additive Manufacturing to Materials Design,” *Coatings 2019, Vol. 9, Page 418*, vol. 9, no. 7, p. 418, Jun. 2019, doi: 10.3390/COATINGS9070418.

[51] L. Nuñez, C. M. Downey, I. J. van Rooyen, I. Charit, and M. R. Maughan, “Analysis of surface roughness in metal directed energy deposition,” *International Journal of Advanced Manufacturing Technology*, 2024, doi: 10.1007/S00170-024-13587-8.

[52] M. Khanzadeh, S. Chowdhury, M. A. Tschopp, H. R. Doude, M. Marufuzzaman, and L. Bian, “In-situ monitoring of melt pool images for porosity prediction in directed energy deposition processes,” *IISE Trans*, vol. 51, no. 5, pp. 437–455, May 2019, doi: 10.1080/24725854.2017.1417656.

[53] S. M. Thompson, L. Bian, N. Shamsaei, and A. Yadollahi, “An overview of Direct Laser Deposition for additive manufacturing; Part I: Transport phenomena, modeling and diagnostics,” *Addit Manuf*, vol. 8, pp. 36–62, Oct. 2015, doi: 10.1016/J.ADDMA.2015.07.001.

[54] B. Jin *et al.*, “A Review of Additive Manufacturing Techniques and Post-Processing for High-Temperature Titanium Alloys,” *Metals 2023, Vol. 13, Page 1327*, vol. 13, no. 8, p. 1327, Jul. 2023, doi: 10.3390/MET13081327.

[55] S. E. Haghighi, H. B. Lu, G. Y. Jian, G. H. Cao, D. Habibi, and L. C. Zhang, “Effect of α" martensite on the microstructure and mechanical properties of beta-type Ti–Fe–Ta alloys,” *Mater Des*, vol. 76, pp. 47–54, 2015, doi: https://doi.org/10.1016/j.matdes.2015.03.028.

[56] Y. J. Liu, Z. Liu, Y. Jiang, G. W. Wang, Y. Yang, and L. C. Zhang, “Gradient in microstructure and mechanical property of selective laser melted AlSi10Mg,” *J Alloys Compd*, vol. 735, pp. 1414–1421, 2018, doi: https://doi.org/10.1016/j.jallcom.2017.11.020.

[57] J. Parthasarathy, B. Starly, S. Raman, and A. Christensen, “Mechanical evaluation of porous titanium (Ti6Al4V) structures with electron beam melting (EBM),” *J Mech Behav Biomed Mater*, vol. 3, no. 3, pp. 249–259, 2010, doi: https://doi.org/10.1016/j.jmbbm.2009.10.006.

[58] L. E. Murr *et al.*, “Metal Fabrication by Additive Manufacturing Using Laser and Electron Beam Melting Technologies,” *J Mater Sci Technol*, vol. 28, no. 1, pp. 1–14, 2012, doi: https://doi.org/10.1016/S1005-0302(12)60016-4.

[59] A. Barbas, A. S. Bonnet, P. Lipinski, R. Pesci, and G. Dubois, “Development and mechanical characterization of porous titanium bone substitutes,” *J Mech Behav Biomed Mater*, vol. 9, pp. 34–44, May 2012, doi: 10.1016/j.jmbbm.2012.01.008.

[60] R. K. Gupta, V. A. Kumar, C. Mathew, and G. S. Rao, “Strain hardening of Titanium alloy Ti6Al4V sheets with prior heat treatment and cold working,” *Materials Science and Engineering: A*, vol. 662, pp. 537–550, Apr. 2016, doi: 10.1016/J.MSEA.2016.03.094.

[61] Z. Fu and C. Körner, “Actual state-of-the-art of electron beam powder bed fusion,” *European Journal of Materials*, vol. 2, no. 1, pp. 54–116, Dec. 2022, doi:

10.1080/26889277.2022.2040342;REQUESTEDJOURNAL:JOURNAL:TEMS20;WGROUP:STRING:PUBLICATION.

[62] J. J. Beaman, D. L. Bourell, C. C. Seepersad, and D. Kovar, "Additive Manufacturing Review: Early Past to Current Practice," *Journal of Manufacturing Science and Engineering, Transactions of the ASME*, vol. 142, no. 11, Nov. 2020, doi: 10.1115/1.4048193.

[63] M. Aristizabal, P. Jamshidi, A. Saboori, S. C. Cox, and M. M. Attallah, "Laser powder bed fusion of a Zr-alloy: Tensile properties and biocompatibility," *Mater Lett*, vol. 259, p. 126897, Jan. 2020, doi: 10.1016/J.MATLET.2019.126897.

[64] S. Vock, B. Klöden, A. Kirchner, T. Weißgärber, and B. Kieback, "Powders for powder bed fusion: a review," *Progress in Additive Manufacturing*, vol. 4, no. 4, pp. 383–397, Dec. 2019, doi: 10.1007/S40964-019-00078-6/TABLES/3.

[65] M. H. Mosallanejad, B. Niroumand, A. Aversa, and A. Saboori, "In-situ alloying in laser-based additive manufacturing processes: A critical review," *J Alloys Compd*, vol. 872, p. 159567, 2021, doi: https://doi.org/10.1016/j.jallcom.2021.159567.

[66] S. Chowdhury *et al.*, "Laser powder bed fusion: a state-of-the-art review of the technology, materials, properties & defects, and numerical modelling," *Journal of Materials Research and Technology*, vol. 20, pp. 2109–2172, 2022, doi: https://doi.org/10.1016/j.jmrt.2022.07.121.

[67] N. D. Dejene and H. G. Lemu, "Current Status and Challenges of Powder Bed Fusion-Based Metal Additive Manufacturing: Literature Review," *Metals (Basel)*, vol. 13, no. 2, 2023, doi: 10.3390/met13020424.

[68] K. L. Tan and S. H. Yeo, "Surface finishing on IN625 additively manufactured surfaces by combined ultrasonic cavitation and abrasion," *Addit Manuf*, vol. 31, p. 100938, Nov. 2019, doi: 10.1016/j.addma.2019.100938.

[69] F. Calignano, O. A. Peverini, G. Addamo, and L. Iuliano, "Accuracy of complex internal channels produced by laser powder bed fusion process," *J Manuf Process*, vol. 54, pp. 48–53, Jun. 2020, doi: 10.1016/J.JMAPRO.2020.02.045.

[70] D. Cooper, M. Stanford, K. Kibble, and G. Gibbons, "Additive Manufacturing for product improvement at Red Bull Technology," *Mater Des*, vol. 41, pp. 226–230, Oct. 2012, doi: 10.1016/j.matdes.2012.05.017.

[71] N. Arun Prasanth and S. H. Yeo, "Controlled hydrodynamic cavitation erosion with abrasive particles for internal surface modification of additive manufactured components," *Wear*, vol. 414–415, pp. 89–100, Nov. 2018, doi: 10.1016/j.wear.2018.08.006.

[72] M. R. Bayoumi and A. K. Abdellatif, "Effect of surface finish on fatigue strength," *Eng Fract Mech*, vol. 51, no. 5, pp. 861–870, Jul. 1995, doi: 10.1016/0013-7944(94)00297-U.

[73] P. Li, D. H. Warner, A. Fatemi, and N. Phan, "Critical assessment of the fatigue performance of additively manufactured Ti–6Al–4V and perspective for future research," *Int J Fatigue*, vol. 85, pp. 130–143, Apr. 2016, doi: 10.1016/J.IJFATIGUE.2015.12.003.

[74] T. M. Mower and M. J. Long, “Mechanical behavior of additive manufactured, powder-bed laser-fused materials,” *Materials Science and Engineering: A*, vol. 651, pp. 198–213, Jan. 2016, doi: 10.1016/J.MSEA.2015.10.068.

[75] W. Shi, Y. Liu, X. Shi, Y. Hou, P. Wang, and G. Song, “Beam Diameter Dependence of Performance in Thick-Layer and High-Power Selective Laser Melting of Ti-6Al-4V,” *Materials 2018, Vol. 11, Page 1237*, vol. 11, no. 7, p. 1237, Jul. 2018, doi: 10.3390/MA11071237.

[76] N. Kang, Y. Li, X. Lin, E. Feng, and W. Huang, “Microstructure and tensile properties of Ti-Mo alloys manufactured via using laser powder bed fusion,” *J Alloys Compd*, vol. 771, pp. 877–884, Jan. 2019, doi: 10.1016/j.jallcom.2018.09.008.

[77] H. Irrinki *et al.*, “Effects of powder characteristics and processing conditions on the corrosion performance of 17-4 PH stainless steel fabricated by laser-powder bed fusion,” *Progress in Additive Manufacturing*, vol. 3, no. 1–2, pp. 39–49, Jun. 2018, doi: 10.1007/S40964-018-0048-0.

[78] Y. Zhang *et al.*, “Additive Manufacturing of Metallic Materials: A Review,” *J Mater Eng Perform*, vol. 27, no. 1, pp. 1–13, Jan. 2018, doi: 10.1007/S11665-017-2747-Y/TABLES/6.

[79] X. Han, H. Zhu, X. Nie, G. Wang, and X. Zeng, “Investigation on Selective Laser Melting AlSi10Mg Cellular Lattice Strut: Molten Pool Morphology, Surface Roughness and Dimensional Accuracy,” *Materials*, vol. 11, no. 3, 2018, doi: 10.3390/ma11030392.

[80] H. Hassanin *et al.*, “Tailoring selective laser melting process for titanium drug-delivering implants with releasing micro-channels,” *Addit Manuf*, vol. 20, pp. 144–155, Mar. 2018, doi: 10.1016/J.ADDMA.2018.01.005.

[81] J. C. Snyder, C. K. Stimpson, K. A. Thole, and D. Mongillo, “Build Direction Effects on Additively Manufactured Channels,” *Proceedings of the ASME Turbo Expo*, vol. 5A, Aug. 2015, doi: 10.1115/GT2015-43935.

[82] Y. Solyaev, L. Rabinskiy, and D. Tokmakov, “Overmelting and closing of thin horizontal channels in AlSi10Mg samples obtained by selective laser melting,” *Addit Manuf*, vol. 30, p. 100847, Dec. 2019, doi: 10.1016/J.ADDMA.2019.100847.

[83] E. Yasa, O. Poyraz, E. U. Solakoglu, G. Akbulut, and S. Oren, “A Study on the Stair Stepping Effect in Direct Metal Laser Sintering of a Nickel-based Superalloy,” *Procedia CIRP*, vol. 45, pp. 175–178, Jan. 2016, doi: 10.1016/J.PROCIR.2016.02.068.

[84] L. W. Hunter, D. Brackett, N. Brierley, J. Yang, and M. M. Attallah, “Assessment of trapped powder removal and inspection strategies for powder bed fusion techniques,” *International Journal of Advanced Manufacturing Technology*, vol. 106, no. 9–10, pp. 4521–4532, Feb. 2020, doi: 10.1007/S00170-020-04930-W/FIGURES/9.

[85] K. Mumtaz and N. Hopkinson, “Top surface and side roughness of Inconel 625 parts processed using selective laser melting,” *Rapid Prototyp J*, vol. 15, no. 2, pp. 96–103, Mar. 2009, doi: 10.1108/13552540910943397.

[86] D. Gu, D. Dai, W. Chen, and H. Chen, “Selective laser melting additive manufacturing of hard-to-process tungsten-based alloy parts with novel crystalline growth morphology and enhanced

performance," *Journal of Manufacturing Science and Engineering, Transactions of the ASME*, vol. 138, no. 8, Aug. 2016, doi: 10.1115/1.4032192.

[87] A. Ghanekar, R. Crawford, and D. Watson, "Optimization of SLS Process Parameters using D-Optimality".

[88] A. Charles, A. Elkaseer, L. Thijs, V. Hagenmeyer, and S. Scholz, "Effect of Process Parameters on the Generated Surface Roughness of Down-Facing Surfaces in Selective Laser Melting," *Applied Sciences 2019, Vol. 9, Page 1256*, vol. 9, no. 6, p. 1256, Mar. 2019, doi: 10.3390/APP9061256.

[89] D. Gu and Y. Shen, "Balling phenomena in direct laser sintering of stainless steel powder: Metallurgical mechanisms and control methods," *Mater Des*, vol. 30, no. 8, pp. 2903–2910, Sep. 2009, doi: 10.1016/J.MATDES.2009.01.013.

[90] N. K. Tolochko *et al.*, "Balling processes during selective laser treatment of powders," *Rapid Prototyp J*, vol. 10, no. 2, pp. 78–87, 2004, doi: 10.1108/13552540410526953.

[91] J. Y. Lee, A. P. Nagalingam, and S. H. Yeo, "A review on the state-of-the-art of surface finishing processes and related ISO/ASTM standards for metal additive manufactured components," *Virtual Phys Prototyp*, vol. 16, no. 1, pp. 68–96, Jan. 2021, doi: 10.1080/17452759.2020.1830346.

[92] A. P. Nagalingam and S. H. Yeo, "Controlled hydrodynamic cavitation erosion with abrasive particles for internal surface modification of additive manufactured components," *Wear*, vol. 414–415, pp. 89–100, Nov. 2018, doi: 10.1016/J.WEAR.2018.08.006.

[93] K. L. Tan and S. H. Yeo, "Surface modification of additive manufactured components by ultrasonic cavitation abrasive finishing," *Wear*, vol. 378–379, pp. 90–95, May 2017, doi: 10.1016/J.WEAR.2017.02.030.

[94] D. Dai and D. Gu, "Tailoring surface quality through mass and momentum transfer modeling using a volume of fluid method in selective laser melting of TiC/AlSi10Mg powder," *Int J Mach Tools Manuf*, vol. 88, pp. 95–107, Jan. 2015, doi: 10.1016/J.IJMACHTOOLS.2014.09.010.

[95] E. Maleki, S. Bagherifard, M. Bandini, and M. Guagliano, "Surface post-treatments for metal additive manufacturing: Progress, challenges, and opportunities," *Addit Manuf*, vol. 37, p. 101619, Jan. 2021, doi: 10.1016/J.ADDMA.2020.101619.

[96] J. P. Gandreddi, A. Kromanis, J. Lungevics, and E. Jost, "Overview of Machinability of Titanium Alloy (Ti6Al4V) and Selection of Machining Parameters," *Latvian Journal of Physics and Technical Sciences*, vol. 60, no. 1, pp. 52–66, Feb. 2023, doi: 10.2478/LPTS-2023-0005.

[97] P. Edwards and M. Ramulu, "Fatigue performance evaluation of selective laser melted Ti–6Al–4V," *Materials Science and Engineering: A*, vol. 598, pp. 327–337, 2014, doi: https://doi.org/10.1016/j.msea.2014.01.041.

[98] M. Rehan, T. He, A. K. Khalil, D. Tahir, W. S. Yip, and S. S. To, "Experimental Investigation of the Micro-Milling of Additively Manufactured Titanium Alloys: Selective Laser Melting and Wrought Ti6Al4V," *Volume 37, Issue 1*, vol. 37, no. 1, Jan. 136AD, doi: 10.1186/s10033-024-01139-w.

[99] A. T. Beaucamp, Y. Namba, P. Charlton, S. Jain, and A. A. Graziano, “Finishing of additively manufactured titanium alloy by shape adaptive grinding (SAG),” *Surf Topogr*, vol. 3, no. 2, p. 024001, Apr. 2015, doi: 10.1088/2051-672X/3/2/024001.

[100] S. Bagehorn, J. Wehr, and H. J. Maier, “Application of mechanical surface finishing processes for roughness reduction and fatigue improvement of additively manufactured Ti-6Al-4V parts,” *Int J Fatigue*, vol. 102, pp. 135–142, Sep. 2017, doi: 10.1016/J.IJFATIGUE.2017.05.008.

[101] H. Masuo *et al.*, “Effects of Defects, Surface Roughness and HIP on Fatigue Strength of Ti-6Al-4V manufactured by Additive Manufacturing,” *Procedia Structural Integrity*, vol. 7, pp. 19–26, Jan. 2017, doi: 10.1016/J.PROSTR.2017.11.055.

[102] A. B. Spierings, T. L. Starr, and K. Wegener, “Fatigue performance of additive manufactured metallic parts,” *Rapid Prototyp J*, vol. 19, no. 2, pp. 88–94, 2013, doi: 10.1108/13552541311302932/FULL/XML.

[103] C. S. Rakurty *et al.*, “Grinding EB-PBF based additive manufactured Ti6Al4V: A surface integrity study,” *Advances in Industrial and Manufacturing Engineering*, vol. 7, p. 100131, 2023, doi: https://doi.org/10.1016/j.aime.2023.100131.

[104] L. Denti, E. Bassoli, A. Gatto, E. Santecchia, and P. Mengucci, “Fatigue life and microstructure of additive manufactured Ti6Al4V after different finishing processes,” *Materials Science and Engineering: A*, vol. 755, pp. 1–9, May 2019, doi: 10.1016/j.msea.2019.03.119.

[105] M. Benedetti *et al.*, “The effect of post-sintering treatments on the fatigue and biological behavior of Ti-6Al-4V ELI parts made by selective laser melting,” *J Mech Behav Biomed Mater*, vol. 71, pp. 295–306, Jul. 2017, doi: 10.1016/J.JMBBM.2017.03.024.

[106] S. Bagehorn, J. Wehr, and H. J. Maier, “Application of mechanical surface finishing processes for roughness reduction and fatigue improvement of additively manufactured Ti-6Al-4V parts,” *Int J Fatigue*, vol. 102, pp. 135–142, Sep. 2017, doi: 10.1016/j.ijfatigue.2017.05.008.

[107] F. Fan, S. Jalui, and G. Manogharan, “Mass finishing of additively manufactured Ti6Al4V parts: An investigation of surface finish dependency on build orientation and processing conditions,” *Volume 35, Pages 439 - 449*, vol. 35, pp. 439–449, Aug. 2023, doi: 10.1016/j.mfglet.2023.08.095.

[108] C. Dowding and A. Borman, “Laser-initiated ablation of materials,” *Laser Surface Engineering: Processes and Applications*, pp. 523–546, Jan. 2015, doi: 10.1016/B978-1-78242-074-3.00022-2.

[109] N. Worts, J. Jones, and J. Squier, “Surface structure modification of additively manufactured titanium components via femtosecond laser micromachining,” *Opt Commun*, vol. 430, pp. 352–357, Jan. 2019, doi: 10.1016/j.optcom.2018.08.055.

[110] O. J. Hildreth, A. R. Nassar, K. R. Chasse, and T. W. Simpson, “Dissolvable metal supports for 3D direct metal printing,” *3D Print Addit Manuf*, vol. 3, no. 2, pp. 91–97, Jun. 2016, doi: 10.1089/3DP.2016.0013;JOURNAL:JOURNAL:3DP;REQUESTEDJOURNAL:JOURNAL:3DP;WGROUP:STRING:PUBLICATION.

[111] G. Pyka *et al.*, “Surface modification of Ti6Al4V open porous structures produced by additive manufacturing,” *Adv Eng Mater*, vol. 14, no. 6, pp. 363–370, 2012, doi: 10.1002/adem.201100344.

[112] G. Pyka, G. Kerckhofs, I. Papantoniou, M. Speirs, J. Schrooten, and M. Wevers, “Surface Roughness and Morphology Customization of Additive Manufactured Open Porous Ti6Al4V Structures,” *Materials 2013, Vol. 6, Pages 4737-4757*, vol. 6, no. 10, pp. 4737–4757, Oct. 2013, doi: 10.3390/MA6104737.

[113] D. Pupillo *et al.*, “Surface treatments on 3D printed Ti6Al4V biomedical plates to enhance corrosion resistance in simulated physiological solutions and under inflammatory conditions,” *Corros Sci*, vol. 240, p. 112451, Nov. 2024, doi: 10.1016/J.CORSCI.2024.112451.

[114] T. Risposi, L. Rusnati, L. Patriarca, A. Hardaker, D. Luczyniec, and S. Beretta, “Fatigue of Ti6Al4V manufactured by PBF-LB: A comparison of failure mechanisms between net-shape and electro-chemically milled surface conditions,” *Eng Fail Anal*, vol. 172, p. 109403, May 2025, doi: 10.1016/j.engfailanal.2025.109403.

[115] B. Wysocki *et al.*, “The influence of chemical polishing of titanium scaffolds on their mechanical strength and in-vitro cell response,” *Materials Science and Engineering: C*, vol. 95, pp. 428–439, Feb. 2019, doi: 10.1016/J.MSEC.2018.04.019.

[116] A. Kołkowska, J. Michalska, R. Zieliński, and W. Simka, “Electrochemical Polishing of Ti and Ti6Al4V Alloy in Non-Aqueous Solution of Sulfuric Acid,” *Materials 2024, Vol. 17, Page 2832*, vol. 17, no. 12, p. 2832, Jun. 2024, doi: 10.3390/MA17122832.

[117] S. Amin Yavari *et al.*, “Bone regeneration performance of surface-treated porous titanium,” *Biomaterials*, vol. 35, no. 24, pp. 6172–6181, 2014, doi: 10.1016/j.biomaterials.2014.04.054.

[118] A. R. McAndrew *et al.*, “Interpass rolling of Ti-6Al-4V wire + arc additively manufactured features for microstructural refinement,” *Addit Manuf*, 2018, doi: 10.1016/j.addma.2018.03.006.

[119] H. Springer *et al.*, “Efficient additive manufacturing production of oxide- and nitride-dispersion-strengthened materials through atmospheric reactions in liquid metal deposition,” *Mater Des*, vol. 111, pp. 60–69, 2016, doi: 10.1016/j.matdes.2016.08.084.

[120] J. R. Hönnige, P. A. Colegrove, S. Ganguly, E. Eimer, S. Kabra, and S. Williams, “Control of residual stress and distortion in aluminium wire + arc additive manufacture with rolling,” *Addit Manuf*, 2018, doi: 10.1016/j.addma.2018.06.015.

[121] J. Gu *et al.*, “Deformation microstructures and strengthening mechanisms for the wire+arc additively manufactured Al-Mg4.5Mn alloy with inter-layer rolling,” *Materials Science and Engineering: A*, 2018, doi: 10.1016/j.msea.2017.11.113.

[122] J. Donoghue, A. A. Antonysamy, F. Martina, P. A. Colegrove, S. W. Williams, and P. B. Prangnell, “The effectiveness of combining rolling deformation with wire-arc additive manufacture on β-grain refinement and texture modification in Ti-6Al-4V,” *Mater Charact*, vol. 114, pp. 103–114, 2016, doi: 10.1016/j.matchar.2016.02.001.

[123] S. Bagehorn, J. Wehr, and H. J. Maier, “Application of mechanical surface finishing processes for roughness reduction and fatigue improvement of additively manufactured Ti-6Al-4V parts,” *Int J Fatigue*, vol. 102, pp. 135–142, Sep. 2017, doi: 10.1016/J.IJFATIGUE.2017.05.008.

[124] P. Tyagi *et al.*, “Reducing the roughness of internal surface of an additive manufacturing produced 316 steel component by chempolishing and electropolishing,” *Addit Manuf*, vol. 25, pp. 32–38, Jan. 2019, doi: 10.1016/J.ADDMA.2018.11.001.

[125] S. Bagherifard, N. Beretta, S. Monti, M. Riccio, M. Bandini, and M. Guagliano, “On the fatigue strength enhancement of additive manufactured AlSi10Mg parts by mechanical and thermal post-processing,” *Mater Des*, vol. 145, pp. 28–41, 2018, doi: 10.1016/j.matdes.2018.02.055.

[126] S. M. Ahmadi *et al.*, “From microstructural design to surface engineering: A tailored approach for improving fatigue life of additively manufactured meta-biomaterials,” *Acta Biomater*, vol. 83, pp. 153–166, Jan. 2019, doi: 10.1016/J.ACTBIO.2018.10.043.

[127] P. Wen *et al.*, “Laser additive manufacturing of Zn metal parts for biodegradable applications: Processing, formation quality and mechanical properties,” *Mater Des*, vol. 155, pp. 36–45, 2018, doi: 10.1016/j.matdes.2018.05.057.

[128] C. Yan, L. Hao, A. Hussein, and P. Young, “Ti-6Al-4V triply periodic minimal surface structures for bone implants fabricated via selective laser melting,” *J Mech Behav Biomed Mater*, vol. 51, pp. 61–73, 2015, doi: 10.1016/j.jmbbm.2015.06.024.

[129] A. Ataee, Y. Li, D. Fraser, G. Song, and C. Wen, “Anisotropic Ti-6Al-4V gyroid scaffolds manufactured by electron beam melting (EBM) for bone implant applications,” *Mater Des*, vol. 137, pp. 345–354, 2018, doi: 10.1016/j.matdes.2017.10.040.

[130] M. Benedetti *et al.*, “The effect of post-sintering treatments on the fatigue and biological behavior of Ti-6Al-4V ELI parts made by selective laser melting,” *J Mech Behav Biomed Mater*, vol. 71, pp. 295–306, Jul. 2017, doi: 10.1016/J.JMBBM.2017.03.024.

[131] E. Maleki and O. Unal, “Shot peening process effects on metallurgical and mechanical properties of 316 L steel via: experimental and neural network modeling,” *Metals and Materials International*, 2019, doi: 10.1007/s12540-019-00448-3.

[132] T. A. Book and M. D. Sangid, “Evaluation of select surface processing techniques for in situ application during the additive manufacturing build process,” *JOM*, vol. 68, pp. 1780–1792, 2016, doi: 10.1007/s11837-016-1897-y.

[133] N. E. Uzan, S. Ramati, R. Shneck, N. Frage, and O. Yeheskel, “On the effect of shot-peening on fatigue resistance of AlSi10Mg specimens fabricated by additive manufacturing using selective laser melting (AM-SLM),” *Addit Manuf*, 2018, doi: 10.1016/j.addma.2018.03.030.

[134] H. Soyama and Y. Okura, “The use of various peening methods to improve the fatigue strength of titanium alloy Ti6Al4V manufactured by electron beam melting,” *AIMS Mater Sci*, vol. 5, pp. 1000–1015, 2018, doi: 10.3934/matersci.2018.5.1000.

[135] M. Sato, O. Takakuwa, M. Nakai, M. Niinomi, F. Takeo, and H. Soyama, “Using cavitation peening to improve the fatigue life of titanium alloy Ti-6Al-4V manufactured by electron beam melting,” *Materials Sciences and Applications*, 2016, doi: 10.4236/msa.2016.74018.

[136] H. Soyama and D. Sanders, “Use of an abrasive water cavitating jet and peening process to improve the fatigue strength of titanium alloy 6Al-4V manufactured by the electron beam powder bed melting (EBPB) additive manufacturing method,” *JOM*, vol. 71, pp. 4311–4318, 2019, doi: 10.1007/s11837-019-03673-8.

[137] R. Karimbaev, Y. S. Pyun, E. Maleki, O. Unal, and A. Amanov, “An improvement in fatigue behavior of AISI 4340 steel by shot peening and ultrasonic nanocrystal surface modification,” *Materials Science and Engineering: A*, vol. 791, p. 139752, 2020, doi: 10.1016/j.msea.2020.139752.

[138] M. Kim *et al.*, “Ultrasonic nanocrystal surface modification of high-speed tool steel (AISI M4) layered via direct energy deposition,” *J Mater Process Technol*, vol. 277, p. 116420, 2020.

[139] C. Ma *et al.*, “Improving surface finish and wear resistance of additive manufactured nickel-titanium by ultrasonic nano-crystal surface modification polishing,” *Materials*, 2020, doi: 10.3390/ma6104737.

[140] M. R. Hill *et al.*, “Recent developments in laser peening technology,” *Advanced Materials and Processes*, 2003.

[141] A. V. Gusarov, M. Pavlov, and I. Smurov, “Residual Stresses at Laser Surface Remelting and Additive Manufacturing,” *Phys Procedia*, vol. 12, no. PART 1, pp. 248–254, Jan. 2011, doi: 10.1016/J.PHPRO.2011.03.032.

[142] J. Vaithilingam, R. D. Goodridge, R. J. M. Hague, S. D. R. Christie, and S. Edmondson, “The effect of laser remelting on the surface chemistry of Ti6al4V components fabricated by selective laser melting,” *J Mater Process Technol*, vol. 232, pp. 1–8, Jun. 2016, doi: 10.1016/J.JMATPROTEC.2016.01.022.

[143] E. Yasa, J. Deckers, and J.-P. Kruth, “The investigation of the influence of laser re-melting on density, surface quality and microstructure of selective laser melting parts,” *Rapid Prototyp J*, vol. 17, no. 5, pp. 312–327, 2011.

[144] E. Yasa and J. P. Kruth, “Microstructural investigation of Selective Laser Melting 316L stainless steel parts exposed to laser re-melting,” *Procedia Eng*, vol. 19, pp. 389–395, Jan. 2011, doi: 10.1016/J.PROENG.2011.11.130.

[145] L. Giorleo, E. Ceretti, and C. Giardini, “Ti Surface Laser Polishing: Effect of Laser Path and Assist Gas,” *Procedia CIRP*, vol. 33, pp. 446–451, Jan. 2015, doi: 10.1016/J.PROCIR.2015.06.102.

[146] Y. Tian *et al.*, “Material interactions in laser polishing powder bed additive manufactured Ti6Al4V components,” *Addit Manuf*, vol. 20, pp. 11–22, Mar. 2018, doi: 10.1016/J.ADDMA.2017.12.010.

[147] M. Kahlin *et al.*, “Improved fatigue strength of additively manufactured Ti6Al4V by surface post processing,” *Int J Fatigue*, vol. 134, p. 105497, May 2020, doi: 10.1016/J.IJFATIGUE.2020.105497.

[148] M. Kahlin *et al.*, “Improved fatigue strength of additively manufactured Ti6Al4V by surface post processing,” *Int J Fatigue*, vol. 134, p. 105497, May 2020, doi: 10.1016/J.IJFATIGUE.2020.105497.

[149] E. Maleki and K. Reza Kashyzadeh, “EFFECTS OF THE HARDENED NICKEL COATING ON THE FATIGUE BEHAVIOR OF CK45 STEEL: EXPERIMENTAL, FINITE ELEMENT METHOD, AND ARTIFICIAL NEURAL NETWORK MODELING,” *Iranian Journal of Materials Science and Engineering*, vol. 14, no. 4, 2017, doi: 10.22068/ijmse.14.4.81.

[150] D. M. Mattox and V. H. Mattox, *Vacuum coating technology*. Springer, 2003.

[151] M. Croes *et al.*, “Antibacterial and immunogenic behavior of silver coatings on additively manufactured porous titanium,” *Acta Biomater*, vol. 81, pp. 315–327, Nov. 2018, doi: 10.1016/J.ACTBIO.2018.09.051.

[152] Y. Kirmanidou *et al.*, "New Ti-alloys and surface modifications to improve the mechanical properties and the biological response to orthopedic and dental implants: A review," *Biomed Res Int*, vol. 2016, no. 1, p. 2908570, 2016.

[153] R. I. Revilla, H. Terryn, and I. De Graeve, "Role of Si in the anodizing behavior of Al-Si alloys: additive manufactured and cast Al-Si10-Mg," *J Electrochem Soc*, vol. 165, no. 9, p. C532, 2018.

[154] H. Kovacı, "Comparison of the microstructural, mechanical and wear properties of plasma oxidized Cp-Ti prepared by laser powder bed fusion additive manufacturing and forging processes," *Surf Coat Technol*, vol. 374, pp. 987–996, Sep. 2019, doi: 10.1016/J.SURFCOAT.2019.06.095.

[155] A. R. Rafieerad, M. R. Ashra, R. Mahmoodian, and A. R. Bushroa, "Surface characterization and corrosion behavior of calcium phosphate-base composite layer on titanium and its alloys via plasma electrolytic oxidation: A review paper," *Materials Science and Engineering: C*, vol. 57, pp. 397–413, Dec. 2015, doi: 10.1016/J.MSEC.2015.07.058.

[156] A. Malakizadi, D. Mallipeddi, S. Dadbakhsh, R. M'Saoubi, and P. Krajnik, "Post-processing of additively manufactured metallic alloys – A review," *Int J Mach Tools Manuf*, vol. 179, p. 103908, Aug. 2022, doi: 10.1016/J.IJMACHTOOLS.2022.103908.

[157] A. du Plessis and E. Macdonald, "Hot isostatic pressing in metal additive manufacturing: X-ray tomography reveals details of pore closure," *Addit Manuf*, vol. 34, p. 101191, Aug. 2020, doi: 10.1016/J.ADDMA.2020.101191.

[158] S. Aguado-Montero, C. Navarro, J. Vázquez, F. Lasagni, S. Slawik, and J. Domínguez, "Fatigue behaviour of PBF additive manufactured TI6AL4V alloy after shot and laser peening," *Int J Fatigue*, vol. 154, p. 106536, Jan. 2022, doi: 10.1016/J.IJFATIGUE.2021.106536.

[159] A. Yadollahi and N. Shamsaei, "Additive manufacturing of fatigue resistant materials: Challenges and opportunities," *Int J Fatigue*, vol. 98, pp. 14–31, May 2017, doi: 10.1016/J.IJFATIGUE.2017.01.001.

[160] M. D. Sangid *et al.*, "Role of heat treatment and build orientation in the microstructure sensitive deformation characteristics of IN718 produced via SLM additive manufacturing," *Addit Manuf*, vol. 22, pp. 479–496, Aug. 2018, doi: 10.1016/J.ADDMA.2018.04.032.

[161] Y. Sun, R. J. Hebert, and M. Aindow, "Effect of heat treatments on microstructural evolution of additively manufactured and wrought 17-4PH stainless steel," *Mater Des*, vol. 156, pp. 429–440, Oct. 2018, doi: 10.1016/J.MATDES.2018.07.015.

[162] W. Tillmann, C. Schaak, J. Nellesen, M. Schaper, M. E. Aydinöz, and K. P. Hoyer, "Hot isostatic pressing of IN718 components manufactured by selective laser melting," *Addit Manuf*, vol. 13, pp. 93–102, Jan. 2017, doi: 10.1016/J.ADDMA.2016.11.006.

[163] A. Yegyan Kumar, Y. Bai, A. Eklund, and C. B. Williams, "The effects of Hot Isostatic Pressing on parts fabricated by binder jetting additive manufacturing," *Addit Manuf*, vol. 24, pp. 115–124, Dec. 2018, doi: 10.1016/J.ADDMA.2018.09.021.

[164] X. Peng, L. Kong, J. Y. H. Fuh, and H. Wang, "A Review of Post-Processing Technologies in Additive Manufacturing," *Journal of Manufacturing and Materials Processing 2021, Vol. 5, Page 38*, vol. 5, no. 2, p. 38, Apr. 2021, doi: 10.3390/JMMP5020038.

[165] D. Lee, T.-Y. So, H.-Y. Yu, G. Kim, and S.-H. Ko, “EffEct of Hot IsostatIc PrEssIng and solutIon HEat trEatmEnt on tHE mIcrostructurE and mEcHanIcal ProPErtIEs of ti-6al-4V alloy manufacturEd by sElEctIVE lasEr mEltIng,” *Arch. Metall. Mater*, vol. 69, pp. 135–139, 2024, doi: 10.24425/amm.2024.147801.

[166] H. Masuo *et al.*, “Influence of defects, surface roughness and HIP on the fatigue strength of Ti-6Al-4V manufactured by additive manufacturing,” *Int J Fatigue*, vol. 117, pp. 163–179, Dec. 2018, doi: 10.1016/J.IJFATIGUE.2018.07.020.

[167] G. Li, W. Zhang, Y. Liu, X. Xiao, D. Song, and Z. Xu, “Effect of Ultrasonic Surface Rolling on Fretting Friction and Wear Properties of Heat-Treated Hot Isostatic Pressing Ti-6Al-4V Alloy,” *J Mater Eng Perform*, vol. 31, no. 5, pp. 3859–3871, May 2022, doi: 10.1007/S11665-021-06483-9/FIGURES/12.

[168] B. K. C. Ganesh, W. Sha, N. Ramanaiah, and A. Krishnaiah, “Effect of shotpeening on sliding wear and tensile behavior of titanium implant alloys,” *Materials & Design (1980-2015)*, vol. 56, pp. 480–486, Apr. 2014, doi: 10.1016/J.MATDES.2013.11.052.

[169] G. L. Wynick and C. J. Boehlert, “Use of electropolishing for enhanced metallic specimen preparation for electron backscatter diffraction analysis,” *Mater Charact*, vol. 55, no. 3, pp. 190–202, Sep. 2005, doi: 10.1016/J.MATCHAR.2005.04.008.

[170] E. Maleki, S. Bagherifard, F. Sabouri, M. Bandini, and M. Guagliano, “Hybrid thermal, mechanical and chemical surface post-treatments for improved fatigue behavior of laser powder bed fusion AlSi10Mg notched samples,” *Surf Coat Technol*, vol. 430, p. 127962, Jan. 2022, doi: 10.1016/J.SURFCOAT.2021.127962.

[171] W. Okuniewski, M. Walczak, and M. Szala, “Effects of Shot Peening and Electropolishing Treatment on the Properties of Additively and Conventionally Manufactured Ti6Al4V Alloy: A Review,” *Materials 2024, Vol. 17, Page 934*, vol. 17, no. 4, p. 934, Feb. 2024, doi: 10.3390/MA17040934.

[172] S. Aguado-Montero, C. Navarro, J. Vázquez, F. Lasagni, S. Slawik, and J. Domínguez, “Fatigue behaviour of PBF additive manufactured TI6AL4V alloy after shot and laser peening,” *Int J Fatigue*, vol. 154, p. 106536, Jan. 2022, doi: 10.1016/J.IJFATIGUE.2021.106536.

[173] A. Diaz, “Surface texture characterization and optimization of metal additive manufacturing-produced components for aerospace applications,” *Additive Manufacturing for the Aerospace Industry*, pp. 341–374, Feb. 2019, doi: 10.1016/B978-0-12-814062-8.00018-2.

[174] D. B. Witkin, D. N. Patel, H. Helvajian, L. Steffeney, and A. Diaz, “Surface Treatment of Powder-Bed Fusion Additive Manufactured Metals for Improved Fatigue Life,” *J Mater Eng Perform*, vol. 28, no. 2, pp. 681–692, Feb. 2019, doi: 10.1007/S11665-018-3732-9/FIGURES/15.

[175] C. Navarro *et al.*, “Effect of surface treatment on the fatigue strength of additive manufactured Ti6Al4V alloy,” vol. 53, pp. 337–344, 2020, doi: 10.3221/IGF-ESIS.53.26.

[176] A. Kumar, Dr. V. Kumar, and Dr. J. Kumar, “A Review on the State of the Art in Wire Electric Discharge Machining (Wedm) Process,” *Anal Biochem*, vol. 109, no. 2, pp. 480–481, 2011, doi: 10.1016/0003-2697(80)90681-8.

[177] A. Mandal and A. R. Dixit, “State of art in wire electrical discharge machining process and performance,” *International Journal of Machining and Machinability of Materials*, vol. 16, no. 1, pp. 1–21, 2014, doi: 10.1504/IJMMM.2014.063918.

[178] L. Feltner, E. Korte, D. F. Bahr, and P. Mort, “Particle size and shape analyses for powder bed additive manufacturing,” *Particuology*, Sep. 2023, doi: 10.1016/J.PARTIC.2023.09.001.

[179] F. H. Kim and S. P. Moylan, “Literature Review of Metal Additive Manufacturing Defects,” *NIST Advanced Manufacturing Series*, pp. 100–116, doi: 10.6028/NIST.AMS.100-16.

[180] T. Ledwaba, B. Mbuyisa, B. Blakey-Milner, C. Steenkamp, and A. Du Plessis, “X-ray computed tomography vs Archimedes method: a head-to-head comparison”, doi: 10.1051/matecconf/202338808002.

[181] T. M. Apostol and M. A. Mnatsakanian, “A Fresh Look at the Method of Archimedes,” *The American Mathematical Monthly*, vol. 111, no. 6, pp. 496–508, Jun. 2004, doi: 10.1080/00029890.2004.11920104.

[182] “ASTM F3637-23 - Standard Guide for Additive Manufacturing of Metal — Finished Part Properties —.” Accessed: Mar. 26, 2025. [Online]. Available: https://standards.iteh.ai/catalog/standards/astm/c8d93bab-a03d-4573-b1e5-7841505d499d/astm-f3637-23?srsltid=AfmBOorcLpvMAdWCDGb0jZPJIWSZVf2vwuxhwh95jq9SKoPfClA23Hx4

[183] P. J. Withers *et al.*, “X-ray computed tomography,” *Nature Reviews Methods Primers 2021 1:1*, vol. 1, no. 1, pp. 1–21, Feb. 2021, doi: 10.1038/s43586-021-00015-4.

[184] G. Michael, “X-ray computed tomography,” *Phys Educ*, vol. 36, no. 6, p. 442, Nov. 2001, doi: 10.1088/0031-9120/36/6/301.

[185] “phoenix v|tome|x s - JWJ NDT.” Accessed: Mar. 27, 2025. [Online]. Available: https://www.jwjndt.com/product/phoenix-vtomex-s/

[186] N. Soro, N. Saintier, H. Attar, and M. S. Dargusch, “Surface and morphological modification of selectively laser melted titanium lattices using a chemical post treatment,” *Surf Coat Technol*, vol. 393, p. 125794, Jul. 2020, doi: 10.1016/J.SURFCOAT.2020.125794.

[187] “TriboIndenter TI 950 : Nanomechanical characterization | Microelectronics Research Center.” Accessed: Jun. 25, 2025. [Online]. Available: https://mrc.utexas.edu/facilities/equipment/triboindenter-ti-950-nanomechanical-characterization

[188] W. C. Oliver and G. M. Pharr, “An improved technique for determining hardness and elastic modulus using load and displacement sensing indentation experiments,” *J Mater Res*, vol. 7, no. 6, pp. 1564–1583, Jun. 1992, doi: 10.1557/JMR.1992.1564/METRICS.

[189] A. Leyland and A. Matthews, “On the significance of the H/E ratio in wear control: a nanocomposite coating approach to optimised tribological behaviour,” *Wear*, vol. 246, no. 1–2, pp. 1–11, Nov. 2000, doi: 10.1016/S0043-1648(00)00488-9.